HHS Public Access

Author manuscript

Annu Rev Biomed Eng. Author manuscript; available in PMC 2020 November 20.

Published in final edited form as:

Annu Rev Biomed Eng. 2019 June 04; 21: 325–364. doi:10.1146/annurev-bioeng-092618-020341.

Digital Manufacturing for Microfluidics

Arman Naderi, **Nirveek Bhattacharjee**, **Albert Folch**

Department of Bioengineering, University of Washington, Seattle, Washington 98195, USA;

Abstract

The microfluidics field is at a critical crossroads. The vast majority of microfluidic devices are presently manufactured using micromolding processes that work very well for a reduced set of biocompatible materials, but the time, cost, and design constraints of micromolding hinder the commercialization of many devices. As a result, the dissemination of microfluidic technology—and its impact on society—is in jeopardy. Digital manufacturing (DM) refers to a family of computer-centered processes that integrate digital three-dimensional (3D) designs, automated (additive or subtractive) fabrication, and device testing in order to increase fabrication efficiency. Importantly, DM enables the inexpensive realization of 3D designs that are impossible or very difficult to mold. The adoption of DM by microfluidic engineers has been slow, likely due to concerns over the resolution of the printers and the biocompatibility of the resins. In this article, we review and discuss the various printer types, resolution, biocompatibility issues, DM microfluidic designs, and the bright future ahead for this promising, fertile field

Keywords

microfluidics; digital manufacturing; 3D printing; stereolithography

1. INTRODUCTION

Digital manufacturing (DM) is an integrated production method in which computers are used for modular three-dimensional (3D) design, performance simulation, automated fabrication, assembly, and quality control (1). With DM, designs can be digitally inspected and adjusted, annotated, and cloud-shared with collaborators, resulting in better design turnaround time, cost, and performance. Vast computer-aided design (CAD) libraries of 3D digital objects are available online for free (see http://grabcad.com/). DM has been applied with great success to improve design efficiency and part performance in the automobile industry and the fields of aeronautics, microelectronics, architecture, sportswear, and biomedical implants, among others (1). Importantly, DM is organically applicable to cloud manufacturing (2), a means of production where fabrication of products is distributed over a network of small-scale, decentralized nodes; unlike present mass manufacturing based on

naderia@uw.edu.

DISCLOSURE STATEMENT

The authors are not aware of any affiliations, memberships, funding, or financial holdings that might be perceived as affecting the objectivity of this review.

rigid supply chains, cloud manufacturing is based on agile small manufacturers that (using DM) can respond swiftly to shifting inventories and market demands (3).

Note that the pressure to shift manufacturing to DM comes from society's push to increase efficiency (and thus decrease cost), rather than from a purely technological advantage. Unlike the situation a couple of decades ago, researchers are now under increasing pressure to translate their inventions into commercial applications, so cost has become an important design constraint. As discussed below, DM techniques are regarded as technically inferior by many microfluidic engineers because achieving resolution and biocompatibility comparable to those of micromolding is an ongoing challenge. In addition, shifting to DM requires investments in equipment and personnel. For these reasons, the microfluidics field has been more reluctant to adopt DM than most other manufacturing industries. As a result, microfluidic chips are still designed using non-DM methods (largely from scratch each time), precursor materials have to be mixed and poured into a mold, and the resulting two-dimensional (2D) layers must be manually aligned and bonded to form the final device.

For many microfluidic laboratories and companies, the non-DM approach has been adequate, at least until recently. The 2D layers are usually constructed by micromolding thermoset or thermoplastic polymers chosen for their high transparency and biocompatibility, such as poly(dimethyl siloxane) (PDMS) (4), poly(methyl methacrylate) (PMMA) (5), cyclic olefin copolymer (COC) (6), and polystyrene (PS) (7). The molding procedures for these polymers have been optimized for microfluidics applications for decades. PDMS has additional favorable physicochemical properties compared with other polymers (gas permeability, high elasticity) and can be replicated repeatedly against photolithographic molds using extremely simple— albeit difficult to automate— procedures [e.g., soft lithography (4, 8)], hence its wide popularity for prototyping among researchers. Compared with PDMS, most thermoplastic polymers used in microfluidics are very inexpensive and can be molded using automated machinery [i.e., by injection molding, thermoforming, or hot embossing (9)], so they have been favored in mass-manufacturing commercial applications. A thermoplastic elastomer exists (10–13); however, most thermoplastics are rigid, which makes them less appropriate than PDMS for the fabrication of microfluidic automation elements such as microvalves and micropumps. Microfluidic platforms based on self-pumping wicking materials such as paper (14–17) and thread (18–23) have been proposed to lower the cost and improve the portability of devices; however, their assay sensitivity and specificity are not improved (24–27).

2. DIGITAL MANUFACTURING TECHNIQUES SUITABLE FOR MICROFLUIDICS

Manufacturing techniques for microfluidics can be divided into three categories: subtractive (Figure 1a), additive (Figure 1b), and molding (also known as formative) (Figure 1c). The first microfluidic devices were produced using subtractive (etching) methods in silicon and glass, derived from methods used to make microelectronic chips (28, 29). Later, researchers used computer numerical control (CNC) milling (30) and laminated object manufacturing [LOM, also called laser-cutting (31)] to fabricate channels, computer-controlled subtractive

manufacturing techniques that were early forms of DM microfluidics. Microfluidic chips can also be made by additive manufacturing (AM, also known as 3D printing, and a form of DM). The use of sacrificial inks (32–34) and of molds that are photolithographically patterned or nickel electroplated (35–37), 3D printed (38–40), or CNC milled (41)—all of which are interesting cost-saving approaches to micromolding that enable the rapid production of difficult-to-mold 3D microfluidic conduits—cannot strictly be categorized as DM and thus is not covered here.

All DM methods share (*a*) the ability to produce a physical device from a digital design file and (*b*) the ability to encode the fabrication process as a set of parameters; importantly, both the design file and the process parameters can be electronically sent to distant collaborators operating a similar machine in order to produce a replica of the local print. There are many DM techniques; however, microfluidics fabrication must meet basic requirements, which help guide the choices of techniques and materials for microfluidics. The first requirement is for the technology of choice to be able to fabricate cavities and channels below ~1 mm in size. A secondary requirement is for the channels to be constructed in a transparent material, so that microscopic observation of experiments becomes possible; for biomedical applications, the material(s) must be biocompatible. Most DM techniques that satisfy the first requirement and thus are acceptable for microfluidics are based on additive manufacturing: stereolithography (SL) (Figure 2a); photopolymer inkjet printing, also called Polyjet or multijet modeling (MJM) (Figure 2b); and fused deposition modeling (FDM), also called thermoplastic extrusion (Figure 2c). DM technologies based on subtractive manufacturing, such as LOM (Figure 2d) and CNC milling, have also been applied to microfluidics with mixed success. We briefly review LOM because it is inexpensive and fast, even though it is limited to 2D-layered geometries, but we do not review CNC milling because, in addition to being restricted to 2D layers, it suffers from very low throughputs (the smallest drill bits are very fragile and cannot cut fast) and therefore has very low utility in microfluidics. All of these techniques except for FDM satisfy the secondary (transparency) requirement; FDM can produce only translucent prints because the material (even if it is initially transparent) is extruded in cylindrical filaments, which inevitably generate surfaces that refract light.

For some laboratories, the adoption of DM technology might depend on its level of user-friendliness. FDM printers are the most user-friendly, and FDM-printed devices require no post-processing. Polyjet printers are also very user-friendly; however, Polyjet-printed devices require some postprocessing. Both SL printers and laser cutters are best operated with some basic knowledge of their principles of operation, and also require postprocessing.

2.1 Stereolithography

SL is a form of 3D printing invented in the 1980s (42) that allows for the assembly-free simultaneous production of quasi-arbitrary 3D shapes in a single polymeric material from a liquid photoresin precursor by means of a focused laser or a digital light projector (DLP). A 3D object is built either by scanning the laser in a 3D path or layer by layer by using selective light exposure to photopolymerize the precursor resin collected in a vat. In the layer-by-layer approach, each layer is projected as an image obtained by digitally sectioning

the 3D object into thin slices (43). In modern desktop systems, the laser is substituted by a (more affordable) DLP (43), and the fluid to be exposed is squeezed into a thin layer by a motorized build plate. The surface along which the photopolymerization of the resin takes place broadly differentiates SL into two approaches (44), commonly referred to as the free-surface approach and the bat configuration.

In DLP-based SL, the *xy* resolution is limited by the size of the projected pixels, and the *z* resolution is determined in part by the resolution of the *z* motor. The minimum cross-sectional area of a microchannel that is attainable by SL depends not only on the laser spot size or pixel resolution but also on the type and viscosity of the resin, which has to be effectively drained from the channels post printing (45). In both laser-based and DLP-based setups, the minimum feature size that is achievable by SL is dependent on the pixel/laser spot size, the absorption spectra of the photoresin, and the diffusivity of the reactants (46). The initial SL patent by Hull (42) was restricted to UV-curable materials; however, recent SL printers incorporate high-intensity focused light-emitting diode (LED) light sources in the visible wavelength (43). For microfluidics, where a transparent resin is desirable, a UV source becomes necessary, since transparent resins feature low absorption (and thus poor resolution) in the visible range (47). The issues of biocompatibility and resolution are discussed in Sections 4.1 and 4.2, respectively.

In SL, a microchannel is built by photopolymerizing the channel walls and then draining the uncured resin from the channel cavity, after the printing is complete (48, 49). This process limits the choice of SL resins, since the final print must be at the very least transparent and, for many applications, biocompatible as well. Figure 3 shows representative microfluidic devices built with SL. The unique 3D capabilities of SL are very appealing for the design of 3D microfluidic mixers that enhance mixing by splitting, combining, and rearranging the flow lines. The first SL-printed microfluidic device, credited to the Renaud group (50) in 2001, was indeed a 3D mixer (Figure 3a). Renaud and colleagues did not report the resin composition; however, their article showed a picture of the transparent walls of the device. Breadmore and colleagues (51) were the first to use a desktop 3D printer (a Miicraft) to produce a variety of microfluidic devices (see the gradient generator used for a Griess test for nitrate in Figure 3b). Recently, the Folch group incorporated UV absorbers such as isopropyl thioxanthone (ITX) to increase *z* resolution; Figure 3c shows a chaotic mixer SL-printed in a transparent, open-source resin formulation, poly(ethylene glycol) diacrylate with a molecular weight (MW) of ~258 (PEG-DA-258), containing the photoinitiator Irgacure 819 and ITX. Kotz et al. SL-printed transparent and chemically resistant passive microfluidic mixers using a fused silica glass nanocomposite (52), as well as a highly fluorinated perfluoropolyether (PFPE) methacrylate resin (53).

DM can reduce production time and costs, so some microfluidic engineers are resorting to SL to produce designs that can also be micromolded. Kadimisetty et al. (54) used a FormLabs SL printer and its clear methacrylate-based resin to develop an inexpensive nucleic acid amplification test for infectious diseases; the device could perform extraction, concentration, and isothermal amplification of nucleic acids in various bodily fluids. SL-based manufacturing allows for easy integration of different functional components, enabling sample-to-answer analysis in so-called unibody point-of-care devices (55). The

Rusling group SL-printed microfluidic arrays and implemented an electrochemiluminescent detection platform to detect DNA damage and genotoxicity of water samples (56), as well as measure prostate cancer biomarker proteins in human serum (57); notably, the total cost of the prostate cancer immunoarray was estimated to be $0.65. Plevniak et al. (58) SL-printed 3D micromixers with 500-μm channels through which blood- and hemoglobin- detecting reagents were driven by capillary pumping; a smartphone was used to measure anemia by colorimetry. The Tanner group (59) reported an SL-printed microfluidic device for the detection of malaria from lysed patient samples by first capturing the malarial parasite protein PfLDH (*Plasmodium falciparum* lactate dehydrogenase) with aptamer-coated magnetic beads and then moving the beads with an external magnet to a separate chamber for a colorimetric assay. Microfluidic devices with slots to incorporate commercially available elements can be SL-printed, and a complete analytical system can be easily realized with minimal manual assembly. For example, the Bau group (60) SL-printed a clamshell-style superhydrophobic device that incorporated a commercial membrane supported on micropillars for separating plasma from large volumes of blood. Tang et al. (61) SL-printed a unibody microfluidic device (with the FormLabs clear resin) that combined a 3D passive mixer and a transparent detection chamber housing a glass slide decorated with capture antibodies for detecting prostate-specific antigen and platelet factor 4. Hampson et al. (62) SL-printed a three-inlet microfluidic-focusing device with grooves perpendicular to the flow direction housing optical fibers for detection and counting of the focused microparticles.

SL printing also enables large-volume preconcentration of samples for detecting low-abundance elements such as pathogens and contaminants. Park et al. (63) reported a microfluidic immunomagnetic preconcentrator for the detection of *Escherichia coli* bacteria from large volumes of blood using ATP luminometry; Su et al. (64) SL-printed a microfluidic preconcentrator for solid-phase extraction and detection of trace elements in seawater by using inductively coupled plasma mass spectrometry. In fact, SL-printed microfluidics has found several applications in separation sciences (65). For example, the Miró group (66) reported a fluidic system for sorptive microextraction of antimicrobials from urine and saliva samples, and Mattio et al. (67) reported a lab-on-valve system to detect and quantify cadmium and lead in water.

2.1.1. The future is digital.—Unlike micromolding, DM's design tools are inherently 3D. The Narayan group (68) pioneered the field of biocompatible microneedles by using two-photon SL and the biocompatible resin Ormocer to create hollow, 800-μm-long microneedles that can penetrate cadaveric porcine adipose tissue (Figure 3d). 3D structures can also be created by assembling modules. Yuen (69) and Yuen et al. (70) first demonstrated SL printing of small interconnecting modules to simplify the fabrication of larger, 3D microfluidic devices (Figure 3e), a fruitful concept that has also been exploited by others (71–73). Yet DM's greatest potential is in building complex microfluidic systems seamlessly by assembling modules in the digital space, a capability already used in the manufacturing of automobiles, planes, microelectronics, and many other products to enhance efficiency [e.g., each module is designed by a different team at a different location using free online collaborative tools (see https://workbench.grabcad.com/)]. This feature has

not been exploited to its full potential in microfluidics, likely because the field is still working on the fundamental issues (e.g., resolution, biocompatibility) and distant microfluidic groups often do not have access to the same resins and/or equivalent 3D printers.

Ohtani et al. (74) used a microstereolithography system (5-μm resolution) to define a 50-μm-diameter channel inside a channel, with which they produced <10-μm-diameter oil-in-water droplets (Figure 3f). Several other groups have attempted to use SL printing to fabricate different emulsion droplet generators, with mixed success (51, 71, 75, 76), perhaps because of resolution issues. A collaboration between the Folch and Jeon groups produced helical channels in Watershed (Figure 3g), a transparent commercial resin, to detect pathogenic bacteria (77, 78). Importantly, these microfluidic devices were created simply, and for the first time, by submitting an electronic 3D CAD file to an online 3D-printing service (45). Such printing services could help democratize access to microfluidic fabrication and standardize the 3D-printer hardware.

PDMS-molded microfluidic systems have traditionally suffered from a lack of standardization in the connectors and interfaces with the outside world. This so-called world-to-chip problem is the cause of inlet leaks, poor yields, and user frustration and is ultimately a barrier to the dissemination and commercialization of PDMS microfluidics. Non-DM microfluidics have been explored to demonstrate modular construction (40, 79–81) and connectors (82–85), but fabrication remains complex (i.e., costly). DM can help address the world-to-chip problem in microfluidics. Medical-grade (industry-standard) connectors—commercially available as injection-molded parts such as Luer-Lock or barb connectors (Figure 3h)—can be downloaded from a free online database and 3D-printed (45), resulting in devices that are more user-friendly and less prone to leaking than their PDMS-molded counterparts. The Warkiani group (86) SL-printed a flow distributor that enabled delivery of diluted blood into individual PDMS spiral channels at uniform flow rates and collection of the separated plasma and blood cells. The Nordin group (87) developed microgaskets in PEG-DA-258 that enable up to 121 reversible chip-to-chip and world-to-chip connections simultaneously at a density of 88 connections per square millimeter. Van den Driesche et al. (88) SL-printed chip holders with reliable fluidic and electric connections using O rings (for fluidic sealing) and spring probes (for electrical connections) that fitted precisely inside the printed holders and could be exchanged without gluing or bonding. They used an EnvisionTec printer and eShell300, a class IIa biocompatible resin used for hearing aid shell manufacturing; however, coating with Parylene-C was necessary to ensure cytocompatibility. SL-printed bioreactors for bacterial cultures (Figure 3i) (89) and osteochondral cell cultures (90) and an oxygen control insert in Watershed for a 24-well dish (91) are other examples of 3D constructs that would be very difficult to mold and that pave the way for 3D-printed mammalian cell culture modular systems that could easily be disseminated to other labs in the near future.

2.1.2. Microfluidic automation in stereolithography.—

By enabling mass parallelization, integrated microfluidic automation minimizes sample consumption, speeds up sample processing, and reduces human labor costs (92). Manz and colleagues (29) introduced integrated microvalves and micropumps in 1993, but their electrokinetic

operation required complex glass-etching processes that required specialized facilities. The advent of PDMS microvalves and micropumps (93–95) in 2000 revolutionized the field of microfluidics and allowed for the miniaturization and automation of a vast array of biomedical assays (96, 97). However, PDMS valve fabrication is currently expensive because it consists of multiple steps (some of which are difficult to automate), including photolithography, molding, bonding, and aligning/assembly of small parts. For this reason, DM is a very good case study for improving manufacturing processes for microfluidic automation.

Researchers have looked for an alternative material to PDMS that is more amenable to manufacturing microfluidic valves. Among the photopolymerizable (and thus 3D-printable) resins, PEG-DA-258 stands out as a very good alternative because it is transparent and biocompatible (for more detail about how PEG-DA-258 was developed as a material, see Section 4.1). Beebe et al. (98) showed that a pH-responsive hydrogel could be photopolymerized inside a microchannel from the mixture of acrylic acid, 2-hydroxyethyl methacrylate, ethylene glycol dimethacrylate, and the photoinitiator Irgacure 651 (3 wt%); the photopolymerized structures were used as pH-responsive microvalves. Additional evidence about the manufacturability of PEG-DA was provided by Doyle and colleagues, who used stop-flow lithography to microfabricate various PEG-DA objects inside microchannels (99–101), including flow sensors (102), biocompatible microstructures (103), and cell-laden guided particles (104). This early research generally used PEG-DA with an MW of ~400–1,000, which polymerizes into a high-water-content porous material (a hydrogel), whereas lower-MW PEG-DA polymerizes into a plastic. Kim et al. (105) were the first to photopolymerize PEG-DA-258 onto a mold to form protein-repellent, impermeable microchannels. The Nordin and Woolley groups molded photopolymerized PEG-DA-258 microvalves (106) and reported the first 3D-printed PEG-DA-258 valves (107). Upon improving the resin formulation and optimizing the concentration of photoinitiator Irgacure 819 (108), these authors 3D-printed smaller (~1-mm-diameter) valves in PEG-DA-258 (109) (Figure 3j); however, the prints contained a colorant additive (Sudan Orange) to increase optical absorption, which rendered the prints orange. Folch and colleagues (110) produced the first transparent valves and pumps in Watershed (Figure 3k), but the valves were necessarily large (~1 cm diameter) because Watershed is a rigid polymer: Its Young's modulus is $E \sim 2{,}146$ MPa (111), versus $E \sim 2$ MPa for PDMS (112) and $E \sim 130$ MPa (106) for PEG-DA-258. Consequently, the Folch group (113) developed a transparent, biocompatible formulation of PEG-DA-258 containing the UV absorber ITX; with a 385-nm- wavelength SL-printer, they 3D-printed 500-μm-diameter Quake-style microvalves (a simple architecture that simplifies plumbing) in 8 × 8 arrays (Figure 3l). Similarly, Nordin and colleagues constructed high-density arrays (up to 9 × 5) of 300-μm-diameter PEG-DA microvalves using a formulation that contains the UV absorber 2-nitrophenyl phenyl sulfide (NPS) (87), although cytocompatibility was not tested. Chan et al. (114) demonstrated manual torque-actuated valves and pumps that were integrated in an SL-printed chip for urine protein colorimetric detection with a smartphone (Figure 3m). Bhattacharjee et al. (115) created an elastomeric resin that can be used with DLP-SL printers and results in PDMS-like prints of cytocompatible microchannels and flexible structures (Figure 3n), although the resolution does not yet permit the printing of microvalves.

2.1.3. Multimaterial stereolithography.—Even though SL is essentially a single-material process, it is possible to perform multimaterial printing (also called coprinting) by exchanging the resin in the vat during the printing process (116–124). Materials are best coprinted if their chemistries are compatible; that is, their solvents should be the same and their polymerized products should chemically bind to one another to provide layer-to-layer continuity. Wicker and colleagues (116) first demonstrated that PEG-DA (of differing MWs) provided an ideal multimaterial system for SL and built an SL apparatus with four vats in a rotating carousel (117, 119). A similar multimaterial SL strategy has been used to fabricate multicellular scaffolds with photocrosslinkable bioinks in tissue engineering (122–125). Turri and colleagues (126) used a single-run multi- material SL to incorporate biofunctional scaffolds (average pore size of 400 μm) of biotinylated glyceryl-dimethacrylate within a microfluidic perfusion channel printed using the commercial transparent resin RF080 (Figure 3o). Folch and colleagues (121) adapted these processes to a commercial DLP-SL printer in order to coprint porous barriers of PEG-DA-700 hydrogel between two microfluidic compartments made of impermeable PEG-DA-258; such devices can be used for biomolecular separations (Figure 3p).

2.2. Polyjet

Polyjet, also known as photopolymer inkjet printing and multijet modeling, is a form of 3D printing that uses an inkjet head to deliver droplets of a photocurable polymer that are rapidly cured by UV light. Polyjet technology was invented and patented in 1999 by Objet, a company now owned by Stratasys. In a similar 3D-printing technique called binder jetting, an inkjet head dispenses a mixture of an aqueous binding agent and a powder, rather than the proprietary Objet/Stratasys inks, to create 3D objects layer by layer; the powder itself acts as the support or sacrificial material.

Polyjet is attractive because the printers are user-friendly and can simultaneously deliver multiple materials with a wide range of material properties (hard and soft plastics, elastomers) and different colors (127), providing combinatorially infinite mixtures of materials. Polyjet printers can build structures at high resolution that are comparatively large (8-inch cube) and have been used to build prototypes with smooth finishes and complex shapes, including manufacturing tools, working gears, and metallic electrodes (128). However, the inkjet formulations used in Polyjet printers are proprietary and expensive, which suppresses innovation. Furthermore, there is concern about poor cytocompatibility, and biofunctionality studies with mammalian systems are lacking (see Section 4.1), so most Polyjet microfluidic researchers have focused on nonbiological applications. For microfluidic fabrication, where overhanging structures or complex shapes require support, the inkjets can deliver a gel-like sacrificial material that may be dissolved (e.g., Stratasys's SUP706, which is soluble in NaOH) after the build is complete; this diffusion-limited step is an important limitation for building small, intricate, 3D microfluidic channels. Clearly, Polyjet will have a bright future when the patents expire and academic developers can start innovating open-source biocompatible and functional resins.

The first Polyjet-printed fluidic device was fabricated in 2010 by Bonyár et al. (129), who devised a disposable, transparent microfluidic mixer and homogenizer (channel size, 1 mm ×

2 mm cross section) for gynecological cervical sample storage and preprocessing (i.e., DNA and protein separation); the reagent and the sample were stored in two reservoirs that could be expelled by pressing with the fingertips for mixing (Figure 4a). These researchers also innovated the ubiquitous NaOH dissolution step. Spence and colleagues (130) used Polyjet printers to fabricate devices for cell-based drug assays containing channels (3 mm × 1.5 mm cross section) with open wells that enabled interfacing with commercially available porous membrane inserts. This design cleverly dodges biocompatibility concerns about the Polyjet prints by incorporating a commercial (biocompatible) well insert as the cell culture surface, thereby minimizing possible exposure to leachates. The design was later used to generate dynamic, in vitro pharmacokinetic profiles and also enables direct access to cells for measurement of cellular pharmacodynamics (Figure 4b) (131). In this application, Polyjet printing allowed for two-material printing: an elastomeric resin (TangoBlack Plus) was used to print gaskets, whereas a clear resin (VeroClear) was used to print the channels. A variation of this design was used for electrochemical detection (132); various electrode materials (platinum, platinum black, carbon, gold, silver) could be easily added to a threaded receiving port printed on the device, enabling a modular approach wherein the electrodes are removable and can be easily repolished for reuse after exposure to biological samples (Figure 4c). A microfluidic channel (375-μm-square cross section) integrated with an electrode in the wall-jet configuration was printed with an Objet Eden printer (using Full Cure 720 resin) and employed for electrochemical detection of catechol (133). The Warkiani group (134) Polyjet-printed a miniature hydrocyclone (an industrial device for high-throughput separation of particles) and used it to sort microalgae (Figure 4d). The Kumacheva group (135) Polyjet-printed a microfluidic-spraying nozzle to generate submicrometer $CaCO_3$ nanoparticles and create conductive patterns of single-walled carbon nanotubes (CNTs) on an insulating substrate. They also 3D-printed a pen-type microfluidic print head to sequentially or simultaneously extrude up to four different shear-thinning gel inks, as well as a microfluidic device to extrude hydrogel and composite polymer sheets (135).

2.2.1. Microfluidic automation in Polyjet.—

Causier et al. (136) Polyjet-printed a bubble pump and a miniaturized NMR cell, both fitted inside the narrow bore of an NMR magnet, in order to reduce the presence of bubbles that degrade field homogeneity in NMR measurements (Figure 4e). Sochol et al. (137) Polyjet-printed integrated fluidic circuits containing both static and dynamic elements with VisiJet M3 Crystal as the photocurable plastic and wax as the sacrificial resin. After printing, they cleaned the wax by first heating the entire printed block to 80°C and then sequentially flowing hot mineral oil and blowing compressed air through the internal channel voids, whose smallest dimensions were ~200 μm. Bellow diaphragms measuring 1–2 cm in diameter and 150 μm in thickness served as the dynamic deformable element and were used in designing fluidic capacitors, diodes, transistors, and a multiflow controller device (Figure 4f).

Walczak et al. (138) reported a 200–300-μm-thick hinged-flap check valve that was 3D-printed with a VisiJet M3 Crystal and had a backward-to-forward flow ratio of ~0.01 at 100 kPa (the valves, however, did not close completely, even at 500 kPa). Ukita et al. (139) fabricated a centrifugal microfluidic device for a smartphone-based colorimetric enzyme-

linked immunosorbent assay (ELISA) by 3D-printing grooves and open chambers, which were then closed with a transparent adhesive tape. The Duan group (140) used dual-material Polyjet printing to build a monolithic double-emulsion generator device. The central coaxial channel was printed with flexible Tango Plus FLX930 and the surrounding rigid structures with VeroClear; the diameter of the flexible coaxial channel could be pneumatically constricted to generate double emulsions with different compositions or with different numbers of droplets. The Ismagilov group (141) cleverly employed the multimaterial printing property of Polyjet printing to build a pumping lid that can be used to pressurize or pull vacuum from the inlets of a microfluidic device (Figure 4g). In another application, the same group built an integrated interlock meter-mix device that accurately aspirates predetermined volumes of clinical urine sample, adds a lysis buffer, and runs it through a 3D static micromixer to prepare the sample for extraction and detection of bacterial DNA (142). The multimaterial printing capability along with the use of a hard plastic (Veroclear) and a flexible elastomer (Tango Plus) ensured leak-proof connections between the solid parts, which were still easy to move by hand.

2.2.2. Other inkjet-based approaches.—

Inkjet printing, from which Polyjet evolved, has attracted the attention of biomedical scientists for a long time. In 2003, the Boland group pioneered the direct inkjet printing of protein solutions (collagen) and endothelial and smooth muscle cells with modified Hewlett-Packard 660C (143) or Canon Bubble Jet printers (144). Sanjana & Fuller (145) inkjet-printed microislands made of a poly-d-lysine/collagen mixture (65-μm-diameter resolution) on a PEG background to selectively attach dissociated rat hippocampal neurons that were electrophysiologically and immunocytochemically normal for up to 10 days in culture compared with control culture. Atala and colleagues (146) used inkjet printing technology to prepare complex heterogeneous tissue constructs that contained multiple cell types.

Polyjet printing has been widely used in the medical sector to create anatomically accurate models for orthopedic (147), cardiac (148), and intracranial (149) surgeries. Biosensors have also benefited from the user-friendliness, speed, high resolution, and advances in ink chemistry and printers (for a review, see Reference 150). However, these advances did not address the basic challenges of creating polymeric channels for microfluidics.

2.3. Fused Deposition Modeling

FDM, also known as thermoplastic extrusion, is a form of 3D printing invented by Crump (151) wherein a heated thermoplastic material is extruded from a motor-driven nozzle head that can move in three dimensions. The material hardens by spontaneous cooling immediately after extrusion. FDM printers are mechanically simple and thus relatively inexpensive and user-friendly. An open-source community of designers in this area has flourished (see, e.g., the Thingiverse website at http://www.thingiverse.com/).

While resolution in FDM still presents a challenge, the technique's biocompatibility and multimaterial versatility are unparalleled. FDM is sold in convenient filament rolls of inexpensive and biocompatible thermoplastic polymers such as acrylonitrile butadiene styrene (ABS), polylactic acid (PLA), polycarbonate, polyethylene terephthalate glycol-

modified, thermoplastic elastomers, thermoplastic polyurethane, PMMA, polypropylene, nylon, polyamide, and polystyrene, among others. Biodegradable, water-soluble, conductive, ferromagnetic, metal-colored, glow-in-the-dark, thermochromic, and/or ceramic plastics are also available. A related FDM strategy, in which liquid precursors such as metallic solutions, hydrogels, or cell-laden solutions are extruded through a nozzlehead, has been employed to create LEDs (152), batteries (153), strain gauges on flexible substrates (154), antennas (155), interconnects (156), and electrodes within biological tissue (157).

Although FDM-printed microfluidics are appealing because they can be created simply by pressing a button, microchannel fabrication with FDM has presented a challenge for several reasons: (*a*) The sizes of the extruded filaments are larger than typical channels used in microfluidics; (*b*) from a topological consideration, it might not be possible to lay down the walls of any arbitrary channel layout in the form of extruded filaments, especially at channel intersections, where joining filament ends can cause leaks; and (*c*) the lack of structural integrity between the layers can result in weak seals (158). To improve structural integrity, one can promote cross-linking of the filaments by γ-irradiation (159) and cause covalent bond formation via the Diels–Alder reaction upon cooling (160).

Given these resolution challenges, many groups have creatively resorted to FDM to print so-called millifluidic channels for a variety of less-resolution-demanding applications. The Cronin group FDM-printed chemical reactionware microreactor devices containing 800-μm-wide channels made of polypropylene and acetoxysilicone polymer (161–163), as well as plug-and-play droplet generators that can generate 300-μm-diameter droplets (164) (Figure 5a). The Bread- more group leveraged the surface roughness generated by the deposition of tubular filaments in FDM printing to enhance mixing in microfluidic channels; mixing was maximized when the filaments were extruded at 60o with respect to the flow direction (165). The Rusling group built microfluidic devices with 800-μm-square channels (printed by extruding polyethylene terephthalate and PLA filaments) for amperometric detection of hydrogen peroxide (Figure 5b) (166), immunoarray-based detection of cancer protein biomarkers (Figure 5c) (167), and electrochemical detection of breast cancer biomarkers (168). The King and Oxman groups (169) demonstrated Golden Gate DNA assembly in FDM-printed fluidics (in some cases using the 3D-printing service Shapeways) with 220-μm-wide channels, 490-nL-volume reactions, and total device costs ranging from a fraction of a dollar to ~$5.00. The Bowser group built a microfluidic free-flow electrophoresis device by assembling (acetone vapor-bonding) two FDM-printed ABS pieces, one containing the channel features for the electrodes (345 μm deep) and the channels (80 μm deep) and the other containing the fluidic connection ports (170). Notably, the fully functional device was fabricated for ~$0.20 in material costs in less than 36 h (of which only 10 min were needed for manual intervention). Morgan et al. (171) created PLA droplet generators and, remarkably, showed that it is possible to observe fluid flow within the 3D-printed PLA devices, either by embedding a glass observation window for microscopy applications (Figure 5d) or by building very thin (i.e., translucent) PLA roofs (Figure 5e, f). The Breadmore group (172) used a dual-extruder FDM printer to build an integrated 400-μm-wide porous barrier (using a composite Lay–Felt filament) separating 700-μm channels made with ABS (Figure 5g); the composite Lay–Felt barrier turned porous after dissolution of the water-soluble component within the barrier. The printing process was interrupted to

embed liquid Griess reagent in one of the channels before building the roof over the channels.

FDM printing has also been used to fabricate microfluidic solid-phase extraction devices for petroleum processing (173). Dolomite's Fluidic Factory FDM printer has been optimized for creating completely sealed 3D microfluidic devices in COC, a solvent-resistant, hard, transparent, medical-grade thermoplastic. However, this printer is significantly more expensive than most FDM printers (see https://www.dolomite-microfluidics.com/).

Several groups have exploited the high biocompatibility and multimaterial capability that FDM has to offer. McAlpine and colleagues (174) used a custom-built FDM printer to fabricate a multimaterial three-chamber device (Figure 5h) to study interactions among neurons, glia, and epithelial cells. The device was built by printing 350-μm-wide polycaprolactone microchannels (for guiding axons), followed by a silicone sealant (for fluidic isolation of the chambers), and finally a trichamber made with polycaprolactone (for keeping the fluidic environments of the neurons, glia, and epithelial cells separate). Parker and colleagues (175) built cardiac organ-on-a-chip devices (Figure 5i) using a multimaterial FDM printer capable of dispensing piezoresistive, high-conductance, viscous PDMS inks, which enabled the integration of soft strain gauge sensors within the device and the study of drug responses and contractile development of human stem cell–derived cardiac tissues for more than 4 weeks. Johnson et al. (176) introduced an approach to the fabrication of personalized (implantable) nerve repair FDM-printed constructs for the regeneration of complex peripheral nerve injuries containing bifurcating sensory and motor nerve pathways (Figure 5j,k). The McAlpine group (177) also FDM-printed implantable core/shell capsules containing payload biomolecules for the light-programmable release of multiplexed gradients. Duarte et al. (178) used FDM to print a monolithic microfluidic device to generate (as well as measure) the size of emulsion droplets in real time. They used a composite CNT-doped PLA filament to print the embedded electrodes and ABS for the rest of the device, including the microchannels.

FDM has been useful for microfluidic fabrication, and reciprocally, microfluidic devices have been useful for FDM-printed hydrogel constructs. A variation of FDM in which a hydrogel solution is extruded through a nozzle has become an important bioprinting technique due to its inherent cytocompatibility (179–182). In 2011, the Khademhosseini and Lee groups (183) invented a PDMS microfluidic device capable of spinning silk microfibers with a digitally encoded chemical composition (Figure 5l). These spatially coded microfibers were used for selective seeding of 3D cell cultures. Seki and colleagues (184) generated micro-organoids of hepatocytes and fibroblasts within alginate hydrogel microfibers that were extruded by a PDMS microfluidic device; the micro-organoid cocultures featured high (~80%) hepatocyte viability over 30 days and revealed enhancement of liver-specific functions such as albumin secretion and urea synthesis as well as expression of hepatocyte-specific genes. A variation of this device enabled the extrusion of stripe-patterned hydrogel sheets of hepatocytes and 3T3 cells, which developed into micro-organoids embedded in the sheets (185). Walus and colleagues (186) incorporated PDMS valves to add programmable multimaterial hydrogel-switching capability. Similarly, the Lewis group (187) developed microfluidic print heads for multimaterial FDM printing of

viscoelastic inks, and Renaud and colleagues (188) developed a micromachined silicon nozzle for FDM printing of hydrogels.

2.4. Laminated Object Manufacturing

LOM is a low-cost technique in which plastic, metal, or ceramic laminates (189, 190) are cut with a laser or a physical plotter tip [i.e., xurography (191)] and aligned, assembled layer by layer, and affixed with glue or chemicals to create 3D objects. Although LOM, unlike most 3D-printing techniques, typically requires assembly steps to build microfluidic channels, the manufacturing process can be fully specified from a digital file, just as in other DM methods. Laser ablation–based microstructuring of polymeric substrates has been used for biomicrofluidic applications (192, 193). The Yager group fabricated microfluidic devices by laminating Mylar sheets for a variety of different applications, such as isoelectric focusing based–protein separation (194), rapid immunoassay (195), electrophoresis (196), cell lysis (197), and protein reconstitution (198). Neils et al. (199) built a complex microfluidic combinatorial mixer by stacking nine layers of Mylar laminates. Duffy et al. (200) assembled a lab-on-a-disk device for phosphate determination in water by laminating laser-cut PMMA sheets for the larger features with intervening plotter-cut adhesive sheets for the microfluidic channels. The Rasooly group (201) built a miniature 96-well ELISA test by assembling five polycarbonate sheets and one PMMA laminate.

Multilayer microfluidic devices have been produced by laminating photolithographically fabricated negative photoresist (SU-8 or polyimide) layers in a process termed lab-on-foil (202). Despite improvements in LOM (203), the method is limited by the production of debris during the cutting or gluing of the layers, which results in obstruction of microchannels, and by the formation of a lip of reflowed plastic on the rim of the channels, which interferes with the sealing of the channel network. Ogilvie et al. (204) developed a method to reduce the impact of this lip formation and reduce the overall surface roughness of PMMA. This method involves exposing PMMA to a solvent vapor of chloroform that induces polymer reflow of a very thin layer of PMMA on its surface and thereby removes rough features.

3. THE LIMITATIONS OF MICROMOLDING APPROACHES ARE THE ADVANTAGES OF DIGITAL MANUFACTURING

Micromolding approaches were introduced to microfluidics in the 1990s as a way to reduce the cost per chip and broaden the spectrum of materials, until then limited to silicon and glass. Thus, micromolding has been an enabling technology for many microfluidic applications that would never have been possible with silicon or glass micromachining. However, as the field has advanced, it has become obvious that micromolding approaches present fundamental limitations that can hinder the progress of microfluidics.

3.1. Physical Versus Digital

In micromolding approaches, (most of) the information to produce the final product is contained in a mold that needs to be physically fabricated, whereas in DM approaches, (most of) the information to make the final product is contained in a digital file. In both cases, the

information is often incomplete and some postprocessing is required. In microfluidics, micromolding was originally conceived to reuse the molds, but the layered approach comes at the price of extra hassles— bonding, alignment, inlet punching—where the fabrication skills of the user largely dictates the success of the fabrication process. As a result, dissemination of micromolded microfluidic technology requires physical transfer of personnel and devices. With DM, device design is fully specified in CAD software, which directly enables finite-element modeling of fluids and materials properties prior to printing. Importantly, in DM, expertise is encoded as a set of parameters that are entered to operate the machine, enabling straightforward transfer of expertise within groups and between distant groups.

3.2. Long Cycle Times

Compared with DM approaches, micromolding approaches are not ideal for prototyping, because making photomasks and molds unnecessarily lengthens the cycle time. In soft lithography, the cycle time (~1 day) is mostly filled by photomask printing, photolithographic processing (i.e., spinning, baking, exposing, and developing the photoresist), and thermal curing of PDMS. In injection molding, the long cycle time (>2 weeks) involves micromachining the mold's metal parts and optimizing the plastic injection conditions that are required for that particular mold. Past the research and development and prototyping phases, in injection molding the initial investment can be spread over a large number of devices, making such approaches popular among microfluidics companies. By contrast, DM is inherently fast (typical cycle time, ~1 h) since it circumvents the steps involved in producing the photomasks and the mold.

3.3. Total Production Costs

Micromolding approaches, in particular injection molding, have traditionally been used to reduce the cost per device. However, injection molding is cost effective only when large numbers of devices are produced, because the technique requires the fabrication of (usually metallic) molds that can sustain the high pressure of molten plastic injected into the molds. With micromolding, microfluidic structures (e.g., a channel, a chamber, or a microvalve) must be fabricated by stacking and bonding at least two layers. This approach limits the complexity of the chips that can be fabricated and raises the cost as chip complexity increases (due to the skilled labor involved in aligning and bonding the chips). The cost of the process makes it difficult for companies to diversify their portfolio. Typically, metal molds can cost between US$15,000 and $100,000, depending on size and feature complexity, so production runs on the order of 100,000 to a million pieces in order to absorb the cost of the molds (and reach an average cost of less than a dollar per device) are common. However, few microfluidic applications involve a market that can sell such large numbers of identical units. Plastic molding methods that are less expensive than injection molding exist, such as thermoforming (202) or hot embossing (9), but they have much lower throughputs (a few dozen devices per day per mold). PDMS molding suffers from a different problem: The photolithographic molds are relatively inexpensive, but the molding procedure is usually based on specialized, costly manual labor (instead of automated procedures, as in injection molding), so the throughput is dismally low—one replication step every few hours is the running average. As a result, no commercially available PDMS microfluidic device

costs less than $100. The more complex the device is, the more expensive it is to produce it. Fluidigm—arguably the most successful microfluidic company—built a facility for automated PDMS fabrication in Singapore, but the cost of building such a facility is beyond the financial power of most microfluidic companies, and their multilayer polymerase chain reaction valve chips sell for more than $500 each. In sum, since launching a microfluidic device requires large investments, the vast majority of microfluidic device concepts that are successful at the academic stage (the so-called killer apps) are not successfully commercialized. By comparison, since DM allows for low-risk sales strategies based on on-demand fabrication and a diverse digital catalog of products (i.e., digital marketplaces), DM might enable the inexpensive launching of (arbitrarily complex) microfluidic devices in the near future.

DM, usually based on additive manufacturing (known as 3D printing), does not have any of the above-described limitations of micromolding technologies. These limitations mean that the production of microfluidic devices by micromolding, while optimized for mass manufacturing, cannot be optimized at the same time for design variety and customization. In other words, so far the commercialization of microfluidics has been restricted to mass-manufactured applications, but there are many other possible applications that could benefit from technologies that do not rely on economies of scale. The economics of 3D printing are well suited for microfluidics because, as opposed to molding approaches, the cost per device does not scale up with its 3D complexity (complexity is free) and is insensitive to the size of the production batch; in other words, 3D printing is ideal for project customization (variety is free) (3). Since more than 90% of the cost of a project can be in the form of salaries, DM should alleviate research costs because most of DM fabrication is automated, enabling projects in low-resource settings with a relatively small capital investment.

4. BARRIERS TO ADOPTION OF DIGITAL MANUFACTURING IN MICROFLUIDICS

DM technologies have disadvantages, which act as barriers to adoption of DM in microfluidics. Although DM, as described above, offers unsurpassable design capabilities (digital, 3D, high variety, speed, low cost, etc.) and promises to fuel the democratization of access to microfluidic technology, many microfluidic researchers (especially those working in bio-related fields) cannot compromise on resolution and biocompatibility. To be adopted by these researchers, DM technology must outcompete high-resolution technology (soft lithography and injection molding) and materials (PDMS and thermoplastics) of highly suitable properties, namely transparency, biocompatibility (both PDMS and thermoplastics), elasticity, oxygen permeability (only PDMS), and so forth. In the following subsections, we identify four major barriers to the adoption of DM in microfluidics.

4.1. First Barrier: Biocompatibility of the Resins

Photopolymerizable resins have been developed for a variety of applications prior to being explored for microfluidics (205). In particular, a wealth of knowledge on photopolymerizable hydrogels (of a variety of MWs) was amassed early on in the fields of tissue engineering and drug delivery. Photopolymerizable hydrogels can be readily

manufactured; are permeable to oxygen, nutrients, and other water-soluble metabolites; and have a consistency similar to that of soft tissues (206–208). Although PEG-DA hydrogels are cell inert, bioactivity can be induced via covalent attachment of cell-adhesion ligands, growth factors, and cytokines to the polymer backbone (209, 210). Also, PEG hydrogels can in principle be rendered biodegradable through the incorporation of a proteolytically degradable unit into the PEG backbone (209, 211). The photopolymerization of hydrogels into complex 3D cell-laden structures has thus become essential for a variety of biomedical fields, including cell biology research (212), biosensors (124, 213), soft robotics (214), tissue engineering (123, 215–220), and implants (221). In a noteworthy example, in 1999 the Hubbell group (222) photoencapsulated porcine islets of Langerhans in PEG-DA (MW ranging from 2,000 to 20,000) and found that the islets were viable and contained insulin after 30 days implantation in Sprague Dawley rats. This landmark study showed that cells can survive the process of PEG-DA photopolymerization and can live inside PEG-DA hydrogels, paving the way toward further investigations on cells and materials. West and colleagues (223, 224) used PEG-DA-3400 to photolithographically pattern cell-laden scaffolds using the photoinitiator 2,2-dimethoxy-2-phenyl-acetophenone (365-nm wavelength). The Wicker group (225) demonstrated SL-printed cell-laden PEG-DA-1000 constructs made using the photoinitiator Irgacure 2959. Ovsianikov et al. (226) found a formulation of PEG-DA-700 that shows high viability with mouse fibroblasts. Zhang & Larsen (227) used the biocompatible photoinitiator lithium phenyl-2,4,6-trimethylbenzoylphosphinate (LAP) (228) to SL-print PEG-DA-700 perfusion channels surrounding a central chamber with live 3T3 fibroblasts embedded in UV-cross-linked gelatin-methacrylate (GelMA). More recently, Brigo et al. (212) used two-photon illumination (with a Nanoscribe) to photopolymerize Gel-MA and PEG-DA-700 into submicrometer-resolution woodpile scaffolds for seeding a human foreskin fibroblast cell line; they synthesized a two-photon photoinitiator (P2CK). Remarkably, the Stampfl (229) group trapped live *C. elegans* in PEG-DA-700 hydrogel woodpile structures by using two-photon SL (Figure 6a).

A few resins have already undergone some biocompatibility certifications, and several groups in collaboration have begun evaluating the biocompatibility of commercially available resins. Very few resins are transparent, so the shopping list for the biomicrofluidic engineer is not very long. An SL resin, Somos Watershed 11122 XC, and MJM resins, VisiJet M3 Crystal and MED610, have been certified as US Pharmacopeial Convention (USP) Class VI or medical-grade plastic. MED610 and Watershed have met more stringent biocompatibility standards—International Standards Organization (ISO) certifications 10993–5 (cytotoxicity) and 10993–10 (irritation and delayed-type hypersensitivity)—and MED610 has also met ISO 10993–3 (genotoxicity), 10993–18 (chemical characterization of organic and aqueous extracts), and 13485 (every batch of material undergoes biocompatibility testing) certifications. Accura 60 has the typical clarity and hardness of polycarbonate, and Asiga's GR-10 is a transparent methacrylate-based resin for dental applications. While rigorous biocompatibility data for Accura 60 are lacking, Ong et al. (230) used it to SL-print microstructures for trapping and culturing viable ~100-μm-diameter spheroids made from patient-derived oral squamous cell carcinoma cells and HepG2 cell

lines. One-month-long fibroblast cultures showed poor (45%) viability due to leachates from GR-10 (231).

Cells can be exposed to Watershed for short periods of time (77, 78, 110), but not for longer durations (232), and Watershed is not permeable to gases. To quantify the toxicity of 3D-printed microfluidics, Wlodkowic and colleagues (233, 234) performed toxicity profiling of common SL, Polyjet, and FDM polymers using five standard invertebrate and invertebrate whole-organism biotests in various evolutionary stages, such as algae, zooplankton, fish embryos, and larvae. They assessed the biocompatibility of four commercially available resins, including two SL resins (Watershed 11122XC and Fototec SLA 7150), one Polyjet resin (VisiJet Crystal), and an ABS FDM filament; after observing key developmental markers in developing zebrafish embryos, the authors concluded that all 3D-printed parts made with these resins were highly toxic to the embryos (234, 235). Zhu et al. (233) observed significant growth inhibition in freshwater microalgae when they were cultured for 48–96 h in water-soluble leachate extracted from all 3D-printed structures made of FDM (ABS, PLA), Polyjet (VisiJet Crystal, VisiJet SL Clear), and SL resins (Watershed 11122 XC, Fototec 7150 Clear, Form 1 Clear). Aqueous extracts from all SL polymers induced 100% mortality of *Daphnia* sp. neonates after 24 h, and all SL and Polyjet prints proved to be significantly toxic to zebrafish embryos. In contrast to these data, both VisiJet Crystal and Watershed meet biocompatibility standard USP Class VI, and Watershed also meets ISO 10993–5 (cytotoxicity), ISO 10993–10 (sensitization), and ISO 10993–10 (irritation) (see http://www.rpsupport.co.uk/downloads/rps_technical_tips_sl/somos_medical_grade_materials_faqs.pdf), which means that they are deemed safe. A possible explanation for this discrepancy is that leaching is a diffusion-based process, so an initially cytotoxic (leaching) print can in principle be rendered cytocompatible after abundant rinsing and/or immobilization of reactants using additional UV exposure.

The development of microneedles proved to be a very productive challenge for the future development of biomicrofluidic systems by SL in general. The microneedles—just like microchannels—had to be both biocompatible and fabricated at very high resolution. The Narayan group SL-printed various materials, including eShell 200 (a urethane dimethacrylate) (236, 237), Ormocer (an organically modified ceramic) (68, 238, 239), PEG-DA-302 (a plastic) (226), and PEG-DA-700 (a hydrogel) (226). Ormocer contains urethane- and thioether (meth)acrylate alkoxysilanes, and the strong covalent bonds between the ceramic and polymer components endow Ormocer with great chemical stability and very low levels of cytotoxicity (240).

The field of restorative dentistry has also been a fertile ground for SL engineers because of its great interest in developing biocompatible photopolymerizable resins. Dental patients seek tooth corrections, which require the customization of crowns, bridges, impression trays, orthodontic models, gingiva masks, surgical templates for implant placement, and various other prosthetic objects. These devices used to be made by machining (241) and molding, but advances in 3D imaging of the oral cavity with intraoral digital scanners, in 3D printers, and in biocompatible resins have enabled a framework for digital dentistry (242–245). Commercially available SL-based platforms can now be used to plan more efficient and personalized treatment; to improve 3D visualization and interaction with the patient; to

minimize prototyping time, costs, and errors; and to verify the design. The cytocompatibility of various commercially available dentistry resins has been reviewed by Milhem and colleagues (240, 246). Unfortunately, the composition of commercial SL resins is rarely available. 3D printing for maxillofacial (247) and cardiothoracic (248) surgeries has experienced parallel advances, although bone reconstruction typically requires metal implants, so these are not reviewed here.

Many microfluidic researchers started looking for alternatives to PDMS well before the manufacturability of PDMS was called into question. The hydrophobic nature of PDMS microchannel surfaces makes them notoriously prone to sequestering hydrophobic molecules (e.g., most small drugs) into the PDMS bulk (249, 250) and to physisorbing proteins onto the walls (251; for a review, see Reference 252). Both phenomena can potentially alter experimental outcomes by changing the target concentrations and partitioning molecules in undesired regions of a microfluidic device. Hydrophobic PDMS surfaces can be rendered hydrophilic [e.g., via an oxygen plasma treatment (253, 254)], but the PDMS surface undergoes a spontaneous hydrophobic recovery in less than 1 h (253). The need to find more biocompatible substrata inspired several groups to develop microfluidic devices in other, more inert materials, such as Teflon (255) and low-MW PEG-DA (105, 106, 256, 257). Unlike Teflon, PEG-DA is straightforward to photopolymerize in water by addition of commercially available, inexpensive photoinitiators. The lowest-MW PEG-DA that can be obtained commercially has an MW of ~258 (PEG-DA-258) and photopolymerizes into an impermeable plastic. The Khademhosseini and Suh groups (105) showed that micromolded PEG-DA-258 and PEG-DA-330 channels do not swell in water for periods of up to 2 weeks (in addition to being protein repellent), whereas PEG-DA-700 and PEG-DA-875 channels exhibit significant swelling and collapse within 5 h of being put into contact with water. Compared with PDMS controls, PEG-DA-258 microchannels display reduced absorption of small hydrophobic dyes such as Rhodamine B (Figure 6b) (256) or Nile Red (Figure 6c) (258) and are protein repellent (Figure 6d) (105, 256). As a word of caution, since Regehr et al. (250) elegantly showed the effect of PDMS monomers leaching on microfluidic cell cultures, it remains to be shown whether leachate-free PEG-DA-258 prints can be produced; if not, the effects of trace amounts of resin (PEG-DA monomer, photoinitiator, etc.) on clinical assays and relevant cell types will need to be evaluated. The Roy group (218) used digital mirror microdevice (DMD)-based SL to demonstrate the attachment of murine marrow-derived progenitor cells to PEG-DA-258 scaffolds (walls, 50 μm; pores, 150 μm) that were derivatized with fibronectin after printing; they used a 4:1 mixture of PEG-DA-258 and methacrylic acid, the photoinitiator Irgacure 2959 (10%), the UV absorber Tinuvin 234 (0.2%), and a UV source of 355-nm wavelength. By adding the photoinitiator Irgacure 819, Folch and colleagues (47) SL-printed transparent PEG-DA-258 petri dishes and microchannels that sustained 2-day cultures of neurons and CHO cells and that allow for fluorescence microscopy (Figure 6e). Thus, PEG-DA-258 might be not only easier and less expensive to manufacture than PDMS but also more beneficial in applications that require multiple drug or protein applications, such as organ-on-a-chip, drug testing, and/or diagnostics.

The success of PDMS in microfluidics, and its steep manufacturing challenges, has inspired many groups to attempt to develop photosensitive elastomeric resins. Previously, researchers

demonstrated photocurable PDMS (for 2D photolithography) (259–262) and PDMS doped with photoinitiators for multiphoton microstereolithography and direct laser writing at ~1–5-μm resolution (263, 264), but the fabrication rates are very slow and the setups are very expensive. A few commercial (FormLabs Flexible, Stratasys Tango Plus, Spot-A-Elastic, Carbon EPU-40, SIL) and open-source (265, 266) elastomeric SL resins exist for desktop SL printers, but none of these feature the transparency, biocompatibility, and elasticity of Sylgard-184 PDMS. Recently, the Folch lab (115) SL-printed PDMS parts (including a microfluidic channel) from a methacrylate-based resin that can be photopolymerized with 385-nm UV light in a desktop SL printer (Figure 3n). This 3D-printable PDMS (3DP-PDMS) has all the advantageous properties of thermally cured (Sylgard-184) PDMS (115).

In summary, several SL resin formulations have been described in the literature that are transparent, cytocompatible, and openly available to the microfluidic engineer, and some groups have made great strides in improving the transparency and resolution of FDM-printed microfluidic devices (which generally do not suffer from biocompatibility issues). Therefore, the biocompatibility barrier is much lower than it was a decade ago. (Biocompatible Polyjet resins are still lacking.) It is important to recognize that, despite these enormous advances, this barrier has not yet disappeared, because none of the SL resins that are ideally suitable for microfluidics are commercially available. Also, many SL printers are sold with schemes (such as single-brand cartridges and preloaded user settings) that discourage the user from testing other resin formulations. In addition, biocompatibility requires postprocessing (the print needs to be thoroughly rinsed in order to remove unreacted monomers and photoinitiator), which means that the print's final performance can be user dependent. Last but not least, some microfluidic engineers might have objections to formulations that retain a slight yellow tint (due to residual photoinitiator; however, the yellow tint disappears with time by photocleavage).

4.2. Second Barrier: Resolution and Cost of the Printers

Note that although high-resolution printers (especially SL printers) exist, they are not as widely accessible to microfluidic engineers as modern desktop 3D printers, so their impact in microfluidics has so far been limited (267). Employing multiphoton optics can increase the resolution of 3D fabrication to submicrometer levels by tightly focusing high-intensity pulsed laser beams to femtoliter volumes (205, 268–271). In multiphoton direct laser writing (DLW, a type of SL), the photosensitive group in a polymer matrix gets excited by absorbing two (or more) photons simultaneously, which can take place only in a volume with the highest photon flux (205). The N-photon absorption rate is an Nth-order process and steeply decreases with distance from the focal plane (205). DLW is essentially a subtractive manufacturing technique (unlike 3D printing) because it requires dissolution of material. Very high-resolution 3D structures can be printed with DLW by moving the tightly focused laser beams in the 3D space. However, the speed of writing is very slow (on the order of a few millimeters per second) (268), and the cost of DLW systems is beyond the budget of a single lab.

Comparing the resolution of the various DM technologies is difficult because of the wide range of printer models available. The resolution limits are best understood in SL, possibly

because it is the oldest DM technique. Importantly, the processes for creating the channel void—which are different in each DM technique—further lower the resolution. As a rule of thumb, the highest microchannel resolutions are achieved with two-photon SL (~1–5 μm), followed by desktop SL systems (~30–50 μm), Polyjet (~50–100 μm), LOM (~100–150 μm), and FDM (~250 μm). The *xy* resolution is a printer setting that cannot be altered by the user (who can, at best, choose to print at a lower resolution than the maximum setting) and is not always comparable to the *z* resolution. For example, the *xy* (vat-plane) resolution in DLP-SL is a function of the projected pixel size, which is dependent on the size of the micromirrors in the DMD chip and the projection distance to the vat plane; the latter determines the patternable area. An Asiga Pico 2 HD, one of the highest-resolution commercial desktop DLP-SL printers available today, is equipped with a 1,080-pixel, 385-nm UV-light, high-definition projector (1,920 × 1,080 pixels), which results in a projected pixel width of 27 μm in *xy* over an area of 52 mm × 29 mm. By comparison, the Miicraft uses a 1,920 × 1,080 pixel DMD to project 30-μm pixels (at a 365-or 405-nm wavelength) over an area of 57 mm × 32 mm. Higher-resolution 4K ultrahigh-definition projectors (4,096 × 2,160 pixels) capable of producing an ~13-μm-wide projected pixel in a similar build area are now in the pipeline and will soon be available for SL printers.

In photopolymerization processes, the *z* resolution is a function of the resin composition—a parameter that can in principle be changed by the user to improve the *z* resolution; however, most Polyjet systems are typically closed, whereas most SL systems allow for user-supplied resins. Since the resin monomer is typically transparent, the *z* resolution is essentially determined by the absorption of the photoinitiator (and that of any other additives) at the printer's wavelength. Thus, for microfluidics applications where transparent prints are desired, it is critical to use a UV wavelength (typically 385 nm or below) in combination with a photoinitiator that is highly transparent in the visible range and highly absorbent in the UV range (47). In general, the absorbance can be explained quantitatively using the Beer–Lambert law (108), where absorbance (*A*), which is defined as the logarithmic ratio between the radiation intensity entering the resin (*I*0) and the radiation intensity emerging from it (*I*), is equal to the product of the radiation path length through the resin (*l*), the concentration of the absorbing species in the resin (*c*), and its molar absorptivity (ε):

$$A \equiv \log_{10}\frac{I_0}{I} = \varepsilon l c \qquad 1.$$

From Equation 1, it is straightforward to show that the depth to which the resin is photopolymerized (*zr*) is linearly related to the logarithm of the exposure time (*tr*) according to the following equation (108):

$$z_r = \left(\frac{1}{2.303\varepsilon c}\right) * \ln\left(\frac{t_r}{T_0}\right) \qquad 2.$$

Thus, the *z* resolution can be improved by increasing the concentration of the photoinitiator (and the concentration of other absorbing species in the resin); however, a high photoinitiator concentration can make the prints appear yellow due to residual absorption by the photoinitiator in the visible range. Alternatively, it is also possible to use a

photosensitizing additive that strongly absorbs at the same wavelength as the photoinitiator and transfers the energy to the photoinitiator. Several UV-absorbing dyes have been used to increase absorption and *z* resolution in microfluidic systems; for example, Sudan I renders the prints deep orange (272), NPS renders them yellow (273), and ITX renders them transparent and cytocompatible (258).

Figure 7 shows notable high-resolution DM contributions of relevance to microfluidics (for a review, see Reference 267). Early on, Galajda & Ormos (274, 275) photopolymerized small polymer structures (made with the UV-curing optical adhesive Norland NOA 63) with two-photon laser illumination and manipulated these micromachines within the fluid by turning the laser tweezers on and off (Figure 7a). The Sun group (276) incorporated ferrofluid resins to fabricate magnetically actuated microturbines in glass microchannels with two-photon SL (Figure 7b). Similarly, Maruo & Inoue (277, 278) designed micropumps that could be optically made and driven with laser tweezers (Figure 7c). The Sun group used DLW to pattern a variety of microfluidic components inside glass microtrenches (which were later capped to form a microchannel), such as “overpasses” for fluids at junctions (Figure 7d) (279) and microsieves (Figure 7e) (280). The Shear group has created high-resolution 3D bovine serum albumin microstructures (281), which have been used as so-called lobster traps for bacterial cells (282) or to capture bacteria and harness their flagellar motion to drive microfluidic flow (283). Using two-photon SL, Lim et al. (284) created a 3D micromixer consisting of a crossing manifold (Figure 7f); however, the micromixer’s performance was very similar to that demonstrated by the Renaud group (50) using (much cheaper) DLP-SL more than 10 years earlier (Figure 3a), which calls into question the cost–benefit rationale of using two-photon SL for building microfluidic systems.

The high cost of two-photon SL systems has prompted researchers to think of alternative ways of pushing the resolution of SL. A noteworthy effort is that of the Dilase 3D by Kloe, Inc. The Dilase 3D is a laser-based SL system specifically designed for microfluidics, with 5-μm resolution in *xyz* and a large patterning volume of 10 cm (*x*) × 10 cm (*y*) × 5 cm (*z*) at laser scanning speeds above 50 mm/s. The Dilase 3D achieves this large patterning by means of a (proprietary) translation stage system that also moves the objectives. Thus, the patterning area is not coupled to the resolution; in fact, the system can switch to high resolution in the middle of a scan only in the areas where it needs fine features, thereby saving printing time. An example of a print made with the Dilase 3D is shown in Figure 7g.

Since some commercial desktop 3D printers now feature *xy* projected pixel sizes below 30 μm, it is possible to print very small microfluidic structures close to the resolution limit of DLP-SL printers with proper design of the resins. Both the Nordin group (109) and the Folch group (113) have used a PEG-DA-258/Irgacure 819 resin mixture to print PEG-DA-258 microvalve arrays and micropumps. To increase absorbance and be able to produce the thin membrane layer inside the valves, Gong et al. (109) added Sudan Orange to the resin mixture, resulting in colored prints, whereas Lee et al. (113) added ITX, a transparent UV absorber. The Folch group has used a desktop SL printer with a projected pixel size of 27 μm to demonstrate one-pixel-wide, 1-mm-tall (aspect ratio, 37:1) microchannels in a PEG-DA-258 resin containing Irgacure 819 photoinitiator and ITX (Figure 7h). The Nordin

group (273) has built an SL system capable of fabricating microfluidic PEG-DA microchannels with a cross section of 18 μm × 20 μm (Figure 7i).

4.3. Third Barrier: Printing Throughput

DM technologies for microfluidics (including SL, Polyjet, FDM, and LOM) were all conceived as layer-by-layer, serial patterning techniques, so the throughputs are notoriously slow when the whole process is taken into account. In the original free-surface design used by earlier (laser-based) 3D Systems SL printers, the resin is photopolymerized by a laser at its topmost surface that interfaces with air. In this configuration, the metal build stage is always submerged in the resin vat and is translated downward into the vat after every layer is printed. In the more recent bat configuration approach (where the part is printed upside down), the resin is photopolymerized against the bottom surface of the vat, but the print has to be mechanically separated from the vat for each layer. The free-surface configuration results in superior structural fidelity, as the additional mechanical separation step of the bat configuration can induce stress fractures or bending of delicate features. However, since oxygen inhibits the process of photopolymerization, the time of curing is faster in the bat configuration, where the reaction happens away from the air–resin interface. A continuous printing strategy based on the bat configuration approach make the bottom plate permeable to oxygen, thereby inhibiting polymerization at the bottom-most layer and preventing the most recently cured resin layer from adhering to the bottom plate; since separation of the built part from the bottom of the vat is no longer needed at every step, the printing speeds can be increased ~100 times (17). DLP-SL systems, unlike laser-based SL systems, enable parallel patterning over large areas, but the mechanical separation step remains the most time-consuming one.

Other DM technologies have similar fundamental constraints. Polyjet is also based on photo-chemical resins that must be UV cured after being inkjet dispensed. Both Polyjet and FDM share with SL their additive, layer-by-layer strategy, which results in a trade-off between resolution and throughput. The throughput is further slowed by the need to postprocess the prints. In SL, uncured resin must be drained from the channel cavity after printing is complete; this process is largely manual and requires substantial knowhow to connect the inlet and outlet without causing spills. Polyjet also requires a postcuring step, although it is automated, and the dissolution of a so-called sacrificial ink, which creates the channel void. LOM, based on laser cutting and therefore a subtractive manufacturing technique, is fast; however, the channels are usually postprocessed with solvents to achieve smooth sidewalls, and assembly takes time as well.

To be fair, the speed of DM technologies must be compared with that of non-DM technologies, taking into account the time savings during the design phase. SL printing an average 5 cm × 5 cm × 1 mm microfluidic device takes ~1 h, independent of the complexity of the design. Fabrication of the same device in PDMS would typically require 1 day, counting high-resolution photomask printing (one mask per layer), photolithographic mold production (one mold per layer), PDMS replica molding (1 molding step per layer), and PDMS device bonding (one bonding step per layer). Fabrication of the same device by injection molding would take ~2 weeks for each (metal) mold (see https://

www.protolabs.com/services/injection-molding/). Clearly, micromolding strategies were devised for creating larger numbers of copies (i.e., long-term throughput) but cannot compete with DM technologies in terms of short-term throughput. Yet some DM technologies (such as continuous printing in SL) are capable of printing parts on the order of minutes, and printing from digital files naturally allows for the adoption of cloud manufacturing strategies that distribute fabrication over large networks of 3D printers.

4.4. Fourth Barrier: Complacency of the "PDMS Road"

Last but not least, an important barrier to adoption of DM in microfluidics comes from within the microfluidics field itself. Many researchers, understandably, have invested much effort and resources in developing their PDMS protocols, and they are satisfied with how they work for their goals: PDMS is very biocompatible and transparent, and they have already optimized PDMS-molding procedures. The PDMS road, after all, has been extremely successful in the field of microfluidics—so why abandon it?

The force that drives researchers to abandon the PDMS road comes from society and from funding agencies, which insist that research findings and devices be ultimately translated into commercial products that benefit the taxpayers who funded the research. Since PDMS is not easily translated into a commercial product—and DM offers a natural route and resins for the commercialization of microfluidics—we believe that the efficiency of the DM road will ultimately (once it successfully addresses the challenges of resolution and widespread access to biocompatible resins) win over by the simple argument of low cost.

5. CONCLUSIONS

DM microfluidic devices are still in their infancy. The first DM microfluidics date from almost two decades ago, but the cost and availability of the printers and the lack of biocompatible resins have slowed down progress until recently. Understandably, the microfluidics community has been slow to adopt DM techniques despite what DM has to offer. Funding agencies' emphasis on translation has highlighted the high-efficiency features of DM (digital 3D design, rapid prototyping, low cost) and spurred efforts to overcome the remaining challenges (resolution, resin biocompatibility, and commercial availability) before DM microfluidics can come of age. DM techniques are easier to learn, implement, and use than micromolding, so it is not uncommon to see undergraduates—both in engineering and in the biomedical sciences—and even high schoolers learning hands-on DM techniques in the lab and entering the university with DM experience. While micromolding skills were focused on the fabrication phase, DM has shifted the user skills to the design phase because DM fabrication is mostly automated. Thus, we envision a future where microfluidic engineers submit designs to specialized DM services that offer a variety of resins and multimaterial printers. Yet there remain big gaps between the capabilities of present 3D printers and the needs of microfluidic engineers—gaps in resolution, in resin biocompatibility, and in multimaterials capabilities—which are the challenges for the next generation of DM students and scientists.

ACKNOWLEDGEMENTS

A.F. received partial support from National Cancer Institute Grant R01 CA181445.

LITERATURE CITED

1. Zhou Z, Xie S, Chen D. 2012 Fundamentals of Digital Manufacturing Science Berlin:Springer
2. Xu X 2012 From cloud computing to cloud manufacturing. Robot. Comput. Integr. Manuf 28:75–86
3. Lipson H, Kurman M. 2013 Fabricated: The New World of 3D Printing Indianapolis:Wiley
4. Xia YN, Whitesides GM. 1998 Softlithography. Angew. Chem. Int. Ed. Engl 37:551
5. Chen Y, Zhang L, Chen G. 2008 Fabrication, modification, and application of poly(methylmethacrylate) microfluidic chips. Electrophoresis 29:1801–14 [PubMed: 18384069]
6. Jena RK, Yue CY, Lam YC. 2012 Microfabrication of cyclic olefin copolymer (COC) based microfluidic devices. Microsyst. Technol 18:159–66
7. Young EWK, Berthier E, Guckenberger DJ, Sackmann E, Lamers C, et al. 2011 Rapid prototyping of arrayed microfluidic systems in polystyrene for cell-based assays. Anal. Chem 83:1408–17 [PubMed: 21261280]
8. McDonald JC, Whitesides GM. 2002 Poly(dimethylsiloxane) as a material for fabricating microfluidic devices. Acc. Chem. Res 35:491–99 [PubMed: 12118988]
9. Becker H, Locascio LE. 2002 Polymer microfluidic devices. Talanta 56:267–87 [PubMed: 18968500]
10. Brassard D, Clime L, Li K, Miville-Godin C, Roy E, Veres T. 2011 3D thermoplastic elastomer microfluidic devices for biological probe immobilization. Lab Chip 11:4099–107 [PubMed: 22041708]
11. Roy E, Galas J-C, Veres T. 2011 Thermoplastic elastomers for microfluidics: towards a high-throughput fabrication method of multilayered microfluidic devices. Lab Chip 11:3193–96 [PubMed: 21796278]
12. Guillemette MD, Roy E, Auger FA, Veres T. 2011 Rapid isothermal substrate microfabrication of a biocompatible thermoplastic elastomer for cellular contact guidance. Acta Biomater 7:2492–98 [PubMed: 21329768]
13. Roy E, Geissler M, Galas J-C, Veres T. 2011 Prototyping of microfluidic systems using a commercial thermoplastic elastomer. Microfluid. Nanofluidics 11:235–44
14. Martinez AW, Phillips ST, Carrilho E, Thomas SW 3rd, Sindi H, Whitesides GM. 2008 Simple telemedicine for developing regions: camera phones and paper-based microfluidic devices for real-time, off-site diagnosis. Anal. Chem 80:3699–707 [PubMed: 18407617]
15. Diao J, Young L, Kim S, Fogarty EA, Heilman SM, et al. 2006 A three-channel microfluidic device for generating static linear gradients and its application to the quantitative analysis of bacterial chemotaxis. Lab Chip 6:381–88 [PubMed: 16511621]
16. Fu E, Ramsey SA, Kauffman P, Lutz B, Yager P. 2011 Transport in two-dimensional paper networks. Microfluid. Nanofluidics 10:29–35 [PubMed: 22140373]
17. He Y, Wu Y, Fu J-Z, Wu W-B. 2015 Fabrication of paper-based microfluidic analysis devices: a review. RSC Adv 5:78109–27
18. Reches M, Mirica KA, Dasgupta R, Dickey MD, Butte MJ, Whitesides GM. 2010 Thread as a matrix for biomedical assays. ACS Appl. Mater. Interfaces 2:1722–28 [PubMed: 20496913]
19. Li X, Tian J, Shen W. 2010 Thread as a versatile material for low-cost microfluidic diagnostics. ACS Appl. Mater. Interfaces 2:1–6 [PubMed: 20356211]
20. Safavieh R, Zhou GZ, Juncker D. 2011 Microfluidics made of yarns and knots: from fundamental properties to simple networks and operations. Lab Chip 11:2618–24 [PubMed: 21677945]
21. Bhandari P, Narahari T, Dendukuri D. 2011 'Fab-Chips': a versatile, fabric-based platform for low-cost, rapid and multiplexed diagnostics. Lab Chip 11:2493–99 [PubMed: 21735030]
22. Nilghaz A, Wicaksono DH, Gustiono D, Abdul Majid FA, Supriyanto E, Abdul Kadir MR. 2012 Flexible microfluidic cloth–based analytical devices using a low-cost wax patterning technique. Lab Chip 12:209–18 [PubMed: 22089026]

23. Nilghaz A, Ballerini DR, Shena W, Shen W, Shena W. 2013 Exploration of microfluidic devices based on multi-filament threads and textiles: a review. Biomicrofluidics 7:51501 [PubMed: 24086179]
24. Yamada K, Shibata H, Suzuki K, Citterio D. 2017 Toward practical application of paper-based microfluidics for medical diagnostics: state-of-the-art and challenges. Lab Chip 17:1206–49 [PubMed: 28251200]
25. Li X, Ballerini DR, Shen W. 2012 A perspective on paper-based microfluidics: current status and future trends. Biomicrofluidics 6:11301 [PubMed: 22662067]
26. Yetisen AK, Akram MS, Lowe CR. 2013 Paper-based microfluidic point-of-care diagnostic devices. Lab Chip 13:2210–51 [PubMed: 23652632]
27. Hu J, Wang S, Wang L, Li F, Pingguan-Murphy B, et al. 2014 Advances in paper-based point-of-care diagnostics. Biosens. Bioelectron 54:585–97 [PubMed: 24333570]
28. Manz A, Harrison DJ, Verpoorte EMJ, Fettinger JC, Paulus A, et al. 1992 Planar chips technology for miniaturization and integration of separation techniques into monitoring systems—capillary electrophoresis on a chip. J. Chromatogr. A 593:253
29. Harrison DJ, Fluri K, Seiler K, Fan Z, Effenhauser CS, Manz A. 1993 Micromachining a miniaturized capillary electrophoresis–based chemical analysis system on a chip. Science 261:895–97 [PubMed: 17783736]
30. Guckenberger DJ, de Groot TE, Wan AMD, Beebe DJ, Young EWK. 2015 Micromilling: a method for ultra-rapid prototyping of plastic microfluidic devices. Lab Chip 15:2364–78 [PubMed: 25906246]
31. Walsh DI III, Kong DS, Murthy SK, Carr PA. 2017 Enabling microfluidics: from cleanrooms to makerspaces. Trends Biotechnol 35:383–92 [PubMed: 28162773]
32. Therriault D, White SR, Lewis JA. 2003 Chaotic mixing in three-dimensional microvascular networks fabricated by direct-write assembly. Nat. Mater 2:265–71 [PubMed: 12690401]
33. Miller JS, Stevens KR, Yang MT, Baker BM, Nguyen D-HT, et al. 2012 Rapid casting of patterned vascular networks for perfusable engineered three-dimensional tissues. Nat. Mater 11:768–74 [PubMed: 22751181]
34. Gelber MK, Bhargava R. 2015 Monolithic multilayer microfluidics via sacrificial molding of 3D-printed isomalt. Lab Chip 15:1736–41 [PubMed: 25671493]
35. Kim DS, Lee SH, Ahn CH, Lee JY, Kwon TH. 2006 Disposable integrated microfluidic biochip for blood typing by plastic microinjection moulding. Lab Chip 6:794–802 [PubMed: 16738733]
36. Hansen TS, Selmeczi D, Larsen NB. 2010 Fast prototyping of injection molded polymer microfluidic chips. J. Micromech. Microeng 20:15020
37. Rajaguru J, Duke M, Au C. 2015 Development of rapid tooling by rapid prototyping technology and electroless nickel plating for low-volume production of plastic parts. Int. J. Adv. Manuf. Technol 78:31–40
38. Hwang Y, Paydar OH, Candler RN. 2015 3D printed molds for non-planar PDMS microfluidic channels. Sens. Actuators A 226:137–42
39. Glick CC, Srimongkol MT, Schwartz AJ, Zhuang WS, Lin JC, et al. 2016 Rapid assembly of multilayer microfluidic structures via 3D-printed transfer molding and bonding. Microsyst. Nanoeng 2:16063 [PubMed: 31057842]
40. Hsieh Y-F, Yang A-S, Chen J-W, Liao S-K, Su T-W, et al. 2014 A Lego®-like swappable fluidic module for bio-chem applications. Sens. Actuators B 204:489–96
41. Lee UN, Su X, Guckenberger DJ, Dostie AM, Zhang T, et al. 2018 Fundamentals of rapid injection molding for microfluidic cell-based assays. Lab Chip 18:496–504 [PubMed: 29309079]
42. Hull C 1988 Stereolithography: plastic prototype from CAD data without tooling. Mod. Cast 78:38
43. Waldbaur A, Rapp H, Länge K, Rapp BE. 2011 Let there be chip—towards rapid prototyping of microfluidic devices: one-step manufacturing processes. Anal. Methods 3:2681
44. Gross BC, Erkal JL, Lock wood SY, Chen C, Spence DM. 2014 Evaluation of 3D printing and its potential impact on biotechnology and the chemical sciences. Anal. Chem 86:3240–53 [PubMed: 24432804]

45. Au AK, Lee W, Folch A. 2014 Mail-order microfluidics: evaluation of stereolithography for the production of microfluidic devices. Lab Chip 14:1294–301 [PubMed: 24510161]
46. Fang N, Sun C, Zhang X. 2004 Diffusion-limited photopolymerization in scanning microstereolithography. Appl. Phys. A 79:1839–42
47. Urrios A, Parra-Cabrera C, Bhattacharjee N, Gonzalez-Suarez AM, Rigat Brugarolas LG, et al. 2016 3D-printing of transparent bio-microfluidic devices in PEG-DA. Lab Chip 16:2287–94 [PubMed: 27217203]
48. Bertsch A, Bernhard P, Vogt C, Renaud P. 2000 Rapid prototyping of small size objects. Rapid Prototyp. J 6:259–266
49. Kang H-W, Lee IH, Cho D-W. 2004 Development of an assembly-free process based on virtual environment for fabricating 3D microfluidic systems using microstereolithography technology. J. Manuf. Sci. Eng 126:766–71
50. Bertsch A, Heimgartner S, Cousseau P, Renaud P. 2001 Static micromixers based on large-scale industrial mixer geometry. Lab Chip 1:56–60 [PubMed: 15100890]
51. Shallan AI, Smejkal P, Corban M, Guijt RM, Breadmore MC. 2014 Cost-effective three-dimensional printing of visibly transparent microchips within minutes. Anal. Chem 86:3124–30 [PubMed: 24512498]
52. Kotz F, Arnold K, Bauer W, Schild D, Keller N, et al. 2017 Three-dimensional printing of transparent fused silica glass. Nature 544:337–39 [PubMed: 28425999]
53. Kotz F, Risch P, Helmer D, Rapp BE. 2018 Highly fluorinated methacrylates for optical 3D printing of microfluidic devices. Micromachines 9:115
54. Kadimisetty K, Song J, Doto AM, Hwang Y, Peng J, et al. 2018 Fully 3D printed integrated reactor array for point-of-care molecular diagnostics. Biosens. Bioelectron 109:156–63 [PubMed: 29550739]
55. Chan HN, Tan MJA, Wu H. 2017 Point-of-care testing: applications of 3D printing. Lab Chip 17:2713–39 [PubMed: 28702608]
56. Kadimisetty K, Malla S, Rusling JF. 2017 Automated 3-D printed arrays to evaluate genotoxic chemistry: e-cigarettes and water samples. ACS Sens 2:670–78 [PubMed: 28723166]
57. Kadimisetty K, Malla S, Bhalerao KS, MosaI M, Bhakta S, et al. 2018 Automated 3D-printed microfluidic array for rapid nanomaterial-enhanced detection of multiple proteins. Anal. Chem 90:7569–77 [PubMed: 29779368]
58. Plevniak K, Campbell M, Myers T, Hodges A, He M. 2016 3D printed auto-mixing chip enables rapid smartphone diagnosis of anemia. Biomicrofluidics 10:17–19
59. Fraser LA, Kinghorn AB, Dirkzwager RM, Liang S, Cheung Y-W, et al. 2018 A portable microfluidic aptamer-tethered enzyme capture (APTEC) biosensor for malaria diagnosis. Biosens. Bioelectron 100:591–96 [PubMed: 29032164]
60. Liu C, Liao S-C, Song J, Mauk MG, Li X, et al. 2016 A high-efficiency superhydrophobic plasma separator. Lab Chip 16:553–60 [PubMed: 26732765]
61. Tang CK, Vaze A, Rusling JF. 2017 Automated 3D-printed unibody immunoarray for chemiluminescence detection of cancer biomarker proteins. Lab Chip 17:484–89 [PubMed: 28067370]
62. Hampson SM, Rowe W, Christie SDR, Platt M. 2018 3D printed microfluidic device with integrated optical sensing for particle analysis. Sens. Actuators B 256:1030–37
63. Park C, Lee J, Kim Y, Kim J, Lee J, Park S. 2017 3D-printed microfluidic magnetic preconcentrator for the detection of bacterial pathogen using an ATP luminometer and antibody-conjugated magnetic nanoparticles. J. Microbiol. Methods 132:128–33 [PubMed: 27923650]
64. Su CK, Peng PJ, Sun YC. 2015 Fully 3D-printed preconcentrator for selective extraction of trace elements in seawater. Anal. Chem 87:6945–50 [PubMed: 26101898]
65. Kalsoom U, Nesterenko PN, Paull B. 2018 Current and future impact of 3D printing on the separation sciences. Trends Anal. Chem 105:492–502
66. Wang H, Cocovi-Solberg DJ, Hu B, Miró M. 2017 3D-printed microflow injection analysis platform for online magnetic nanoparticle sorptive extraction of antimicrobials in biological specimens as a front end to liquid chromatographic assays. Anal. Chem 89:12541–49 [PubMed: 29039944]

67. Mattio E, Robert-Peillard F, Vassalo L, Branger C, Margaillan A, et al. 2018 3D-printed lab-on-valve for fluorescent determination of cadmium and lead in water. Talanta 183:201–8 [PubMed: 29567165]
68. Ovsianikov A, Chichkov B, Mente P, Monteiro-Piviere NA, Doraiswamy A, Narayan RJ. 2007 Two photon polymerization of polymer–ceramic hybrid materials for transdermal drug delivery. Int. J. Appl. Ceram. Technol 4:22–29
69. Yuen PK. 2008 SmartBuild—a truly plug-n-play modular microfluidic system. LabChip 8:1374–78
70. Yuen PK, Bliss JT, Thompson CC, Peterson RC. 2009 Multidimensional modular microfluidic system. Lab Chip 9:3303–5 [PubMed: 19865740]
71. Bhargava KC, Thompson B, Malmstadt N. 2014 Discrete elements for 3D microfluidics. PNAS 111:15013–18 [PubMed: 25246553]
72. Lee KG, Park KJ, Seok S, Kim DH, Park JY, et al. 2014 3D printed modules for integrated microfluidic devices. RSC Adv 4:32876–80
73. Nie J, Gao G, Qiu J-J, Sun M, Liu A, et al. 2018 3D printed Lego®-like modular microfluidic devices based on capillary driving. Biofabrication 10:035001 [PubMed: 29417931]
74. Ohtani K, Tsuchiya M, Sugiyama H, Katakura T, Hayakawa M, Kanai T. 2014 Surface treatment of flow channels in microfluidic devices fabricated by stereolithography. J. Oleo Sci 63:93–96 [PubMed: 24389798]
75. Femmer T, Jans A, Eswein R, Anwar N, Moeller M, et al. 2015 High-throughput generation of emulsions and microgels in parallelized microfluidic drop-makers prepared by rapid prototyping. ACS Appl. Mater. Interfaces 7:12635–38 [PubMed: 26040198]
76. Zhang JM, Aguirre-Pablo AA, Li EQ, Buttner U, Thoroddsen ST. 2016 Droplet generation in cross-flow for cost-effective 3D-printed ‘plug-and-play’ microfluidic devices. RSC Adv 6:81120–29
77. Lee W, Kwon D, Chung B, Jung GY, Au A, et al. 2014 Ultrarapid detection of pathogenic bacteria using a 3D immunomagnetic flow assay. Anal. Chem 86:6683–88 [PubMed: 24856003]
78. Lee W, Kwon D, Choi W, Jung GY, Au AK, et al. 2015 3D-printed microfluidic device for the detection of pathogenic bacteria using size-based separation in helical channel with trapezoid cross-section. Sci. Rep 5:7717 [PubMed: 25578942]
79. Lim J, Maes F, Taly V, Baret JC. 2014 The microfluidic puzzle: chip-oriented rapid prototyping. Lab Chip 14:1669–72 [PubMed: 24658639]
80. Owens CE, Hart AJ. 2017 High-precision modular microfluidics by micromilling of interlocking injection-molded blocks. Lab Chip 18:890–901
81. Toh AGG, Wang Z, Wang Z. 2016 Modular membrane valves for universal integration within thermoplastic devices. Microfluid. Nanofluidics 20:85
82. Chen A, Pan T. 2011 Fit-to-flow (F2F) interconnects: universal reversible adhesive-free microfluidic adaptors for lab-on-a-chip systems. Lab Chip 11:727–32 [PubMed: 21109877]
83. Wilhelm E, Neumann C, Duttenhofer T, Pires L, Rapp BE. 2013 Connecting microfluidic chips using a chemically inert, reversible, multichannel chip-to-world-interface. Lab Chip 13:4343–51 [PubMed: 24056989]
84. Scott A, Au AK, Vinckenbosch E, Folch A. 2013 A microfluidic D-subminiature connector. Lab Chip 13:2036–39 [PubMed: 23584282]
85. Cooksey GA, Sip CG, Folch A. 2009 A multi-purpose microfluidic perfusion system with combinatorial choice of inputs, mixtures, gradient patterns, and flow rates. Lab Chip 9:417–26 [PubMed: 19156291]
86. Rafeie M, Zhang J, Asadnia M, Li W, Warkiani ME. 2016 Multiplexing slanted spiral microchannels for ultra-fast blood plasma separation. Lab Chip 16:2791–802 [PubMed: 27377196]
87. Gong H, Woolley AT, Nordin GP. 2018 3D printed high density, reversible, chip-to-chip microfluidic interconnects. Lab Chip 18:639–47 [PubMed: 29355276]
88. Van Den Driesche S, Lucklum F, Bunge F, Vellekoop MJ. 2018 3D printing solutions for microfluidic chip-to-world connections. Micromachines 9:71

89. Robinson CD, Auchtung JM, Collins J, Britton RA. 2014 Epidemic *Clostridium difficile* strains demonstrate increased competitive fitness compared to nonepidemic isolates. Infect. Immun 82:2815–25 [PubMed: 24733099]
90. Nichols DA, SondhI S, Little SR, Zunino P, Gottardi R. 2018 Design and validation of an osteochondral bioreactor for the screening of treatments for osteoarthritis. Biomed. Microdevices 20:18 [PubMed: 29445972]
91. Brennan MD, Rexius-Hall ML, Eddington DT. 2015 A 3D-printed oxygen control insert for a 24-well plate. PLOS ONE 10:e0137631 [PubMed: 26360882]
92. Au AK, Lai H, Utela BR, Folch A. 2011 Microvalves and micropumps for BioMEMS. Micromachines 2:179–220
93. Unger MA. 2000 Monolithic microfabricated valves and pumps by multilayer softlithography. Science 288:113–16 [PubMed: 10753110]
94. Thorsen T, Maerkl SJ, Quake SR. 2002 Microfluidic large-scale integration. Science 298:580–84 [PubMed: 12351675]
95. Hosokawa K, Maeda R. 2000 A pneumatically-actuated three-way microvalve fabricated with poly-dimethylsiloxane using the membrane transfer technique. J. Micromech. Microeng 10:415
96. Hong JW, Chen Y, Anderson WF, Quake SR. 2006 Molecular biology on a microfluidic chip. J. Phys. Condens. Matter 18:S691–701
97. Folch A 2013 Introduction to BioMEMS Boca Raton, FL:CRC
98. Beebe DJ, Moore JS, Bauer JM, Yu Q, Liu RH, et al. 2000 Functional hydrogel structures for autonomous flow control inside microfluidic channels. Nature 404:588–90 [PubMed: 10766238]
99. Dendukuri D, Pregibon DC, Collins J, Hatton TA, Doyle PS. 2006 Continuous-flow lithography for high-throughput microparticle synthesis. Nat. Mater 5:365–69 [PubMed: 16604080]
100. Dendukuri D, Gu SS, Pregibon DC, Hatton TA, Doyle PS. 2007 Stop-flow lithography in a microfluidic device. Lab Chip 7:818–28 [PubMed: 17593999]
101. Bong KW, Pregibon DC, Doyle PS. 2009 Lock release lithography for 3D and composite microparticles. Lab Chip 9:863–66 [PubMed: 19294294]
102. Attia R, Pregibon DC, Doyle PS, Viovy J-L, Bartolo D. 2009 Soft microflow sensors. Lab Chip 9:1213–18 [PubMed: 19370239]
103. Cheung YK, Gillette BM, Zhong M, Ramcharan S, Sia SK. 2007 Direct patterning of composite biocompatible microstructures using microfluidics. Lab Chip 7:574–79 [PubMed: 17476375]
104. Chung SE, Park W, Shin S, Lee SA, Kwon S. 2008 Guided and fluidic self-assembly of microstructures using railed microfluidic channels. Nat. Mater 7:581–87 [PubMed: 18552850]
105. Kim P, Jeong HE, Khademhosseini A, Suh KY. 2006 Fabrication of non-biofouling polyethylene glycol micro- and nanochannels by ultraviolet-assisted irreversible sealing. Lab Chip 6:1432–37 [PubMed: 17066166]
106. Rogers CI, Oxborrow JB, Anderson RR, Tsai L-F, Nordin GP, et al. 2014 Microfluidic valves made from polymerized polyethylene glycol diacrylate. Sens. Actuators B 191:438–44
107. Rogers CI, Qaderi K, Woolley AT, Nordin GP. 2015 3D printed microfluidic devices with integrated valves. Biomicrofluidics 9:16501
108. Gong H, Beauchamp M, Perry S, Woolley AT, Nordin GP. 2015 Optical approach to resin formulation for 3D printed microfluidics. RSC Adv 5:106621–32 [PubMed: 26744624]
109. Gong H, Woolley AT, Nordin GP. 2016 High density 3D printed microfluidic valves, pumps, and multiplexers. Lab Chip 16:2450–58 [PubMed: 27242064]
110. Au AK, Bhattacharjee N, Horowitz LF, Chang TC, Folch A. 2015 3D-printed microfluidic automation. Lab Chip 15:1934–41 [PubMed: 25738695]
111. Chantarapanich N, Puttawibul P, Jeamwatthanachai P, Sittheriseripratip LK, Sucharitpwatskul S, Laohaprapanon A. 2011 Optimal matrix size for analysis of tissue engineering scaffold stiffness: a finite element study In Proceedings of the 4th Biomedical Engineering International Conference, pp. 104–7. Piscataway, NJ: IEEE
112. Wang Z, Volinsky AA, Gallant ND. 2014 Crosslinking effect on polydimethylsiloxane elastic modulus measured by custom-built compression instrument. J. Appl. Polym. Sci 131:41050

113. Lee Y-S, Bhattacharjee N, Folch A. 2018 Lab on a chip 3D-printed Quake-style microvalves and micropumps. Lab Chip 18:1207–14 [PubMed: 29553156]
114. Chan HN, Shu Y, Xiong B, Chen Y, Chen Y, et al. 2016 Simple, cost-effective 3D printed microfluidic components for disposable, point-of-care colorimetric analysis. ACS Sens 1:227–34
115. Bhattacharjee N, Parra-Cabrera C, Kim YT, Kuo AP, Folch A. 2018 Desktop-stereolithography 3D-printing of a poly(dimethylsiloxane)-based material with Sylgard-184 properties. Adv. Mater 30:e1800001 [PubMed: 29656459]
116. Arcaute K, Mann B, Wicker R. 2010 Stereolithography of spatially controlled multi-material bioactive poly(ethylene glycol) scaffolds. Acta Biomater 6:1047–54 [PubMed: 19683602]
117. Choi JW, MacDonald E, Wicker R. 2010 Multi-material microstereolithography. Int. J. Adv. Manuf. Technol 49:543–51
118. Kim H, Choi J, Wicker R. 2010 Scheduling and process planning for multiple material stereolithography. Rapid Prototyp. J 16:232–40
119. Choi JW, Kim HC, Wicker R. 2011 Multimaterial stereolithography. J. Mater. Process. Technol 211:318–28
120. MacDonald E, Wicker R. 2016 Multiprocess 3D printing for increasing component functionality. Science 353:aaf2093 [PubMed: 27708075]
121. Kim YT, Castro K, Bhattacharjee N, Folch A. 2018 Digital manufacturing of selective porous barriers in microchannels using multi-material stereolithography. Micromachines 9:125
122. Chan V, Zorlutuna P, Jeong JH, Kong H, Bashir R. 2010 Three-dimensional photopatterning of hydrogels using stereolithography for long-term cell encapsulation. Lab Chip 10:2062–70 [PubMed: 20603661]
123. Lu Y, Mapili G, Suhali G, Chen S, Roy K. 2006 A digital micro-mirror device–based system for the microfabrication of complex, spatially patterned tissue engineering scaffolds. J. Biomed. Mater. Res. A 77:396–405 [PubMed: 16444679]
124. Chan V, Jeong JH, Bajaj P, Collens M, Saif T, et al. 2012 Multi-material bio-fabrication of hydrogel cantilevers and actuators with stereolithography. Lab Chip 12:88–98 [PubMed: 22124724]
125. Miri AK, Nieto D, Iglesias L, Goodarzi Hosseinabadi H, Maharjan S, et al. 2018 Microfluidics-enabled multimaterial maskless stereolithographic bioprinting. Adv. Mater 30:e1800242 [PubMed: 29737048]
126. Credi C, Griffini G, Levi M, Turri S. 2018 Biotinylated photopolymers for 3D-printed unibody lab-on-a-chip optical platforms. Small 14:1702831
127. Pilipović A, Raos P, Šercer M. 2009 Experimental analysis of properties of materials for rapid prototyping. Int. J. Adv. Manuf. Technol 40:105–15
128. Bucella SG, Nava G, Vishunubhatla KC, Caironi M. 2013 High-resolution direct-writing of metallic electrodes on flexible substrates for high performance organic field effect transistors. Org. Electron 14:2249–56
129. Bonyár A, Sántha H, Ring B, Varga M, Kovács JZ, Harsányi G. 2010 3D rapid prototyping technology (RPT) as a powerful tool in microfluidic development. Proc. Eng 5:291–94
130. Anderson KB, Lockwood SY, Martin RS, Spence DM. 2013 A 3D printed fluidic device that enables integrated features. Anal. Chem 85:5622–26 [PubMed: 23687961]
131. Lockwood SY, Meisel JE, Monsma FJ, Spence DM. 2016 A diffusion-based and dynamic 3D-printed device that enables parallel in vitro pharmacokinetic profiling of molecules. Anal. Chem 88:1864–70 [PubMed: 26727249]
132. Erkal JL, Selimovic A, Gross BC, Lockwood SY, Walton EL, et al. 2014 3D printed microfluidic devices with integrated versatile and reusable electrodes. Lab Chip 14:2023–32 [PubMed: 24763966]
133. Munshi AS, Martin RS. 2016 Microchip-based electrochemical detection using a 3-D printed wall-jet electrode device. Analyst 141:862–69 [PubMed: 26649363]
134. Shakeel SM, Rafeie M, Henderson R, Vandamme D, Asadnia M, Ebrahimi Warkiani M. 2017 A 3D-printed mini-hydrocyclone for high throughput particle separation: application to primary harvesting of microalgae. Lab Chip 17:2459–69 [PubMed: 28695927]

135. Alizadehgiashi M, Gevorkian A, Tebbe M, Seo M, Prince E, Kumacheva E. 2018 3D-printed microfluidic devices for materials science. Adv. Mater. Technol 3:1800068
136. Causier A, Carret G, Boutin C, Berthelot T, Berthault P. 2015 3D-printed system optimizing dissolution of hyperpolarized gaseous species for micro-sized NMR. Lab Chip 15:2049–54 [PubMed: 25805248]
137. Sochol RD, Sweet E, Glick CC, Venkatesh S, Avetisyan A, et al. 2016 3D printed microfluidic circuitry via multijet-based additive manufacturing. Lab Chip 16:668–78 [PubMed: 26725379]
138. Walczak R, Adamski K, Lizanets D. 2017 Inkjet 3D printed check microvalve. J. Micromech. Microeng 27:47002
139. Ukita Y, Utsumi Y, Takamura Y. 2016 Direct digital manufacturing of a mini-centrifuge-driven centrifugal microfluidic device and demonstration of a smartphone-based colorimetric enzyme-linked immunosorbent assay. Anal. Methods 8:256–62
140. Ji Q, Zhang JM, Liu Y, Li X, Lv P, et al. 2018 A modular microfluidic device via multimaterial 3D printing for emulsion generation. Sci. Rep 8:479 [PubMed: 29323219]
141. Begolo S, Zhukov DV, Selck DA, Li L, Ismagilov RF. 2014 The pumping lid: investigating multi-material 3D printing for equipment-free, programmable generation of positive and negative pressures for microfluidic applications. Lab Chip 14:4616–28 [PubMed: 25231706]
142. Jue E, Schoepp NG, Witters D, Ismagilov RF. 2016 Evaluating 3D printing to solve the sample-to-device interface for LRS and POC diagnostics: example of an interlock meter-mix device for metering and lysing clinical urine samples. Lab Chip 16:1852–60 [PubMed: 27122199]
143. Wilson WC, Boland T. 2003 Cell and organ printing. 1: Protein and cell printers. Anat. Rec. A272:491–96
144. Roth EA, Xu T, Das M, Gregory C, Hickman JJ, Boland T. 2004 Inkjet printing for high-throughput cell patterning. Biomaterials 25:3707–15 [PubMed: 15020146]
145. Sanjana NE, Fuller SB. 2004 A fast flexible inkjet printing method for patterning dissociated neurons in culture. J. Neurosci. Methods 136:151–63 [PubMed: 15183267]
146. Xu T, Zhao W, Zhu JM, Albanna MZ, Yoo JJ, Atala A. 2013 Complex heterogeneous tissue constructs containing multiple cell types prepared by inkjet printing technology. Biomaterials 34:130–39 [PubMed: 23063369]
147. Ahn DG, Lee JY, Yang DY. 2006 Rapid prototyping and reverse engineering application for orthopedic surgery planning. J. Mech. Sci. Technol 20:19–28
148. Cheng YL, Chen SJ. 2006 Manufacturing of cardiac models through rapid prototyping technology for surgery planning. Mater. Sci. Forum 505–507:1063–68
149. Erbano BO, Opolski AC, Olandoski M, Foggiatto JA, Kubrusly LF, et al. 2013 Rapid prototyping of three-dimensional biomodels as an adjuvant in the surgical planning for intracranial aneurysms. Acta Cir. Bras 28:756–61 [PubMed: 24316741]
150. Li J, Rossignol F, Macdonald J. 2015 Inkjet printing for biosensor fabrication: combining chemistry and technology for advanced manufacturing. Lab Chip 15:2538–58 [PubMed: 25953427]
151. Crump SS. 1989 Apparatus and method for creating three-dimensional objects US Patent 5,121,329A
152. Kong YL, Tamargo IA, Kim H, Johnson BN, Gupta MK, et al. 2014 3D printed quantum dot light-emitting diodes. Nano Lett 14:7017–23 [PubMed: 25360485]
153. Sun K, Wei T-S, Ahn BY, Seo JY, Dillon SJ, Lewis JA. 2013 3D printing of interdigitated Li-ion microbattery architectures. Adv. Mater 25:4539–43 [PubMed: 23776158]
154. Muth JT, Vogt DM, Truby RL, Mengüç Y, Kolesky DB, et al. 2014 Embedded 3D printing of strain sensors within highly stretchable elastomers. Adv. Mater 26:6307–12 [PubMed: 24934143]
155. Adams JJ, Duoss EB, Malkowski TF, Motala MJ, Ahn BY, et al. 2011 Conformal printing of electrically small antennas on three-dimensional surfaces. Adv. Mater 23:1335–40 [PubMed: 21400592]
156. Lopes JA, MacDonald E, Wicker RB. 2012 Integrating stereolithography and direct print technologies for 3D structural electronics fabrication. Rapid Prototyp. J 18:129–43

157. Mannoor MS, Jiang Z, James T, Kong YL, Malatesta KA, et al. 2013 3D printed bionic ears. Nano Lett 13:2634–39 [PubMed: 23635097]
158. Capel AJ, Edmondson S, Christie SDR, Goodridge RD, Bibb RJ, Thurstans M. 2013 Design and additive manufacture for flow chemistry. Lab Chip 13:4583–90 [PubMed: 24100659]
159. Shaffer S, Yang K, Vargas J, DiPrima MA, Voit W. 2014 On reducing anisotropy in 3D printed polymers via ionizing radiation. Polymer 55:5969–79
160. Stansbury JW, Idacavage MJ. 2016 3D printing with polymers: challenges among expanding options and opportunities. Dent. Mater 32:54–64 [PubMed: 26494268]
161. Kitson PJ, Rosnes MH, Sans V, Dragone V, Cronin L. 2012 Configurable 3D-printed millifluidic and microfluidic 'lab on a chip' reactionware devices. Lab Chip 12:3267–71 [PubMed: 22875258]
162. Kitson PJ, Glatzel S, Chen W, Lin CG, Song YF, Cronin L. 2016 3D printing of versatile reactionware for chemical synthesis. Nat. Protoc 11:920–36 [PubMed: 27077333]
163. Symes MD, Kitson PJ, Yan J, Richmond CJ, Cooper GJT, et al. 2012 Integrated 3D-printed reactionware for chemical synthesis and analysis. Nat. Chem 4:349–54 [PubMed: 22522253]
164. Tsuda S, Jaffery H, Hezwani M, Robbins PJ, Yoshida M, Cronin L. 2015 Customizable 3Dprinted 'plug and play' millifluidic devices for programmable fluidics. PLOS ONE 10:e0141640 [PubMed: 26558389]
165. Li F, Macdonald NP, Guijt RM, Breadmore MC. 2017 Using printing orientation for tuning fluidic behavior in microfluidic chips made by fused deposition modeling 3D printing. Anal. Chem 89:12805–11 [PubMed: 29048159]
166. Bishop GW, Satterwhite JE, Bhakta S, Kadimisetty K, Gillette KM, et al. 2015 3D-printed fluidic devices for nanoparticle preparation and flow-injection amperometry using integrated Prussian blue nanoparticle-modified electrodes. Anal. Chem 87:5437–43 [PubMed: 25901660]
167. Kadimisetty K, Mosa IM, Malla S, Satterwhite-Warden JE, Kuhns TM, et al. 2016 3D-printed supercapacitor-powered electrochemiluminescent protein immunoarray. Biosens. Bioelectron 77:188–93 [PubMed: 26406460]
168. Carvajal S, Fera SN, Jones AL, Baldo TA, MosaI M, et al. 2018 Disposable inkjet-printed electrochemical platform for detection of clinically relevant HER-2 breast cancer biomarker. Biosens. Bioelectron 104:158–62 [PubMed: 29331430]
169. Patrick WG, Nielsen AAK, Keating SJ, Levy TJ, Wang C-W, et al. 2015 DNA assembly in 3D printed fluidics. PLOS ONE 10:e0143636 [PubMed: 26716448]
170. Anciaux SK, Geiger M, Bowser MT. 2016 3D printed micro free-flow electrophoresis device. Anal. Chem 88:7675–82 [PubMed: 27377354]
171. Morgan AJL, Hidalgo San Jose L, Jamieson WD, Wymant JM, Song B, et al. 2016 Simple and versatile 3D printed microfluidics using fused filament fabrication. PLOS ONE 11:e0152023 [PubMed: 27050661]
172. Li F, Smejkal P, Macdonald NP, Guijt RM, Breadmore MC. 2017 One-step fabrication of a microfluidic device with an integrated membrane and embedded reagents by multimaterial 3D printing. Anal. Chem 89:4701–7 [PubMed: 28322552]
173. Kataoka ÉM, Murer RC, Santos JM, Carvalho RM, Eberlin MN, et al. 2017 Simple, expendable, 3D-printed microfluidic systems for sample preparation of petroleum. Anal. Chem 89:3460–67 [PubMed: 28230979]
174. Johnson BN, Lancaster KZ, HogueI B, Meng F, Kong YL, et al. 2016 3D printed nervous system on a chip. Lab Chip 16:1393–400 [PubMed: 26669842]
175. Lind JU, Lancaster KZ, HogueI B, Meng F, Kong YL, et al. 2017 Instrumented cardiac microphysiological devices via multimaterial three-dimensional printing. Nat. Mater 16:303–8 [PubMed: 27775708]
176. Johnson BN, Lancaster KZ, Zhen G, He J, Gupta MK, et al. 2015 3D printed anatomical nerve regeneration pathways. Adv. Funct. Mater 25:6205–17 [PubMed: 26924958]
177. Gupta MK, Meng F, Johnson BN, Kong YL, Tian L, et al. 2015 3D printed programmable release capsules. Nano Lett 15:5321–29 [PubMed: 26042472]

178. Duarte LC, Chagas CLS, Ribeiro LEB, Coltro WKT. 2017 3D printing of microfluidic devices with embedded sensing electrodes for generating and measuring the size of microdroplets based on contactless conductivity detection. Sens. Actuators B 251:427–32

179. Arslan-Yildiz A, El Assal R, Chen P, Guven S, Inci F, Demirci U. 2016 Towards artificial tissue models: past, present, and future of 3D bioprinting. Biofabrication 8:014103 [PubMed: 26930133]

180. Mandrycky C, Wang Z, Kim K, Kim D-H. 2016 3D bioprinting for engineering complex tissues. Biotechnol. Adv 34:422–34 [PubMed: 26724184]

181. Stanton MM, Samitier J, Sanchez S. 2015 Bioprinting of 3Dhydrogels. Lab Chip 15:3111–15 [PubMed: 26066320]

182. Pereira RF, Bártolo PJ. 2015 3D bioprinting of photocrosslinkable hydrogel constructs. J. Appl. Polym. Sci 132:42458

183. Kang E, Jeong GS, Choi YY, Lee KH, Khademhosseini A, Lee SH. 2011 Digitally tunable physicochemical coding of material composition and topography in continuous microfibres. Nat. Mater 10:877–83 [PubMed: 21892177]

184. Yamada M, Utoh R, Ohashi K, Tatsumi K, Yamato M, et al. 2012 Controlled formation of heterotypic hepatic micro-organoids in anisotropic hydrogel microfibers for long-term preservation of liver-specific functions. Biomaterials 33:8304–15 [PubMed: 22906609]

185. Kobayashi A, Yamakoshi K, Yajima Y, Utoh R, Yamada M, Seki M. 2013 Preparation of stripe-patterned heterogeneous hydrogel sheets using microfluidic devices for high-density coculture of hepatocytes and fibroblasts. J. Biosci. Bioeng 116:761–67 [PubMed: 23845912]

186. Beyer S, Mohamed T, Walus K. 2013 A microfluidics based 3D bioprinter with on-the-fly multimaterial switching capability In Proceedings of the 17th International Conference on Miniaturized Systems for Chemistry and Life Sciences, pp. 176–78. Washington, DC: Chem. Biol. Microsyst. Soc.

187. Hardin JO, Ober TJ, Valentine AD, Lewis JA. 2015 Microfluidic printheads for multimaterial 3Dprinting of viscoelastic inks. Adv. Mater 27:3279–84 [PubMed: 25885762]

188. Serex L, Bertsch A, Renaud P. 2018 Microfluidics: a new layer of control for extrusion-based 3D printing. Micromachines 9:86

189. Himmer T, Nakagawa T, Anzai M. 1999 Lamination of metal sheets. Comput. Ind 39:27–33

190. Obikawa T, Yoshino M, Shinozuka J. 1999 Sheet steel lamination for rapid manufacturing. J. Mater. Process. Technol 89/90:171–76

191. Bartholomeusz DA, Boutte RW, Andrade JD. 2005 Xurography: rapid prototyping of microstructures using a cutting plotter. J. Microelectromechanical Syst 14:1364–74

192. Malek CGK. 2006 Laser processing for bio-microfluidics applications (part II). Anal.Bioanal. Chem 385:1362–69 [PubMed: 16773302]

193. Weigl BH, Bardell R, Schulte T, Battrell F, Hayenga J. 2001 Design and rapid prototyping of thin-film laminate-based microfluidic devices. Biomed. Microdevices 3:267–74

194. Macounová K, Cabrera CR, Holl MR, Yager P. 2000 Generation of natural pH gradients in microfluidic channels for use in isoelectric focusing. Anal. Chem 72:3745–51 [PubMed: 10959958]

195. Hatch A, Kamholz AE, Hawkins KR, Munson MS, Schilling EA, et al. 2001 A rapid diffusion immunoassay in a T-sensor. Nat. Biotechnol 19:461–65 [PubMed: 11329017]

196. Munson MS, Cabrera CR, Yager P. 2002 Passive electrophoresis in microchannels using liquid junction potentials. Electrophoresis 23:2642–52 [PubMed: 12210168]

197. Schilling EA, Kamholz AE, Yager P. 2002 Cell lysis and protein extraction in a microfluidic device with detection by a fluorogenic enzyme assay. Anal. Chem 74:1798–804 [PubMed: 11985310]

198. Garcia E, Kirkham JR, Hatch AV, Hawkins KR, Yager P. 2004 Controlled microfluidic reconstitution of functional protein from an anhydrous storage depot. Lab Chip 4:78–82 [PubMed: 15007445]

199. Neils C, Tyree Z, Finlayson B, Folch A. 2004 Combinatorial mixing of microfluidic streams. LabChip 4:342–50

200. Duffy G, Maguire I, Heery B, Nwankire C, Ducrée J, Regan F. 2017 PhosphaSense: a fully integrated, portable lab-on-a-disc device for phosphate determination in water. Sens. Actuators B 246:1085–91

201. Sun S, Yang M, Kostov Y, Rasooly A. 2010 ELISA-LOC: lab-on-a-chip for enzyme-linked immunodetection. Lab Chip 10:2093–100 [PubMed: 20544092]

202. Focke M, Kosse D, Müller C, Reinecke H, Zengerle R, von Stetten F. 2010 Lab-on-a-foil: microfluidics on thin and flexible films. Lab Chip 10:1365–86 [PubMed: 20369211]

203. Cho I, Lee K, Choi W, Song Y-A. 2000 Development of a new sheet deposition type rapid prototyping system. Int. J. Mach. Tools Manuf 40:1813–29

204. OgilvieI RG, Sieben VJ, Floquet CFA, Zmijan R, Mowlem MC, Morgan H. 2010 Reduction of surface roughness for optical quality microfluidic devices in PMMA and COC. J. Micromech. Microeng 20:65016

205. Malinauskas M, Farsari M, Piskarskas A, Juodkazis S. 2013 Ultrafast laser nanostructuring of photopolymers: a decade of advances. Phys. Rep 533:1–31

206. Nguyen KT, West JL. 2002 Photopolymerizable hydrogels for tissue engineering applications. Biomaterials 23:4307–14 [PubMed: 12219820]

207. Khademhosseini A, Langer R. 2007 Microengineered hydrogels for tissue engineering. Biomaterials 28:5087–92 [PubMed: 17707502]

208. Knipe JM, Peppas NA. 2014 Multi-responsive hydrogels for drug delivery and tissue engineering applications. Regen. Biomater 1:57–65 [PubMed: 26816625]

209. Mann BK, Gobin AS, Tsai AT, Schmedlen RH, West JL. 2001 Smooth muscle cell grow thin photopolymerized hydrogels with cell adhesive and proteolytically degradable domains: synthetic ECM analogs for tissue engineering. Biomaterials 22:3045–51 [PubMed: 11575479]

210. Mann BK, Schmedlen RH, West JL. 2001 Tethered-TGF-β increases extracellular matrix production of vascular smooth muscle cells. Biomaterials 22:439–44 [PubMed: 11214754]

211. Sawhney AS, Pathak CP, Hubbell JA. 1993 Bioerodible hydrogels based on photopolymerized poly(ethylene glycol)-co-poly(α-hydroxy acid) diacrylate macromers. Macromolecules 26:581–87

212. Brigo L, Urciuolo A, Giulitti S, Della Giustina G, Tromayer M, et al. 2017 3D high-resolution two-photon crosslinked hydrogel structures for biological studies. Acta Biomater 55:373–84 [PubMed: 28351679]

213. Park K, Jang J, Irimia D, Sturgis J, Lee J, et al. 2008 'Living cantilever arrays' for characterization of mass of single live cells in fluids. Lab Chip 8:1034–41 [PubMed: 18584076]

214. Cvetkovic C, Raman R, Chan V, Williams BJ, Tolish M, et al. 2014 Three-dimensionally printed biological machines powered by skeletal muscle. PNAS 111:10125–30 [PubMed: 24982152]

215. Gauvin R, Chen YC, Lee JW, Soman P, Zorlutuna P, et al. 2012 Microfabrication of complex porous tissue engineering scaffolds using 3D projection stereolithography. Biomaterials 33:3824–34 [PubMed: 22365811]

216. Soman P, Chung PH, Zhang AP, Chen SC. 2013 Digital microfabrication of user-defined 3D microstructures in cell-laden hydrogels. Biotechnol. Bioeng 110:3038–47 [PubMed: 23686741]

217. Cha C, Soman P, Zhu W, Nikkah M, Camci-Unal G, et al. 2014 Structural reinforcement of cell-laden hydrogels with microfabricated three dimensional scaffolds. Biomater. Sci 2:703–9 [PubMed: 24778793]

218. Han L-HH, Mapili G, Chen S, Roy K. 2008 Projection microfabrication of three-dimensional scaffolds for tissue engineering. J. Manuf. Sci. Eng 130:21005

219. Fozdar DY, Lee JY, Schmidt CE, Chen S. 2010 Hippocampal neurons respond uniquely to topographies of various sizes and shapes. Biofabrication 2:035005 [PubMed: 20823503]

220. Drury JL, Mooney DJ. 2003 Hydrogels for tissue engineering: scaffold design variables and applications. Biomaterials 24:4337–51 [PubMed: 12922147]

221. Sharma B, Fermanian S, Gibson M, Unterman S, Herzka DA, et al. 2013 Human cartilage repair with a photoreactive adhesive-hydrogel composite. Sci. Transl. Med 5:167ra6

222. Cruise GM, Hegre OD, Lamberti FV, Hager SR, Hill R, et al. 1999 In vitro and in vivo performance of porcine islets encapsulated in interfacially photopolymerized poly(ethylene glycol) diacrylate mem- branes. Cell Transplant 8:293–306 [PubMed: 10442742]

223. Hahn MS, Taite LJ, Moon JJ, Rowland MC, Ruffino KA, West JL. 2006 Photolithographic patterning of polyethylene glycol hydrogels. Biomaterials 27:2519–24 [PubMed: 16375965]

224. Tsang VL, Chen AA, Cho LM, Jadin KD, Sah RL, et al. 2007 Fabrication of 3D hepatic tissues by additive photopatterning of cellular hydrogels. FASEB J 21:790–801 [PubMed: 17197384]

225. Arcaute K, Mann BK, Wicker RB. 2006 Stereolithography of three-dimensional bioactive poly(ethylene glycol) constructs with encapsulated cells. Ann. Biomed. Eng 34:1429–41 [PubMed: 16897421]

226. Ovsianikov A, Malinauskas M, Schlie S, Chichkov B, Gittard S, et al. 2011 Three-dimensional laser micro- and nano-structuring of acrylated poly(ethylene glycol) materials and evaluation of their cytoxicity for tissue engineering applications. Acta Biomater 7:967–74 [PubMed: 20977947]

227. Zhang R, Larsen NB. 2017 Stereolithographic hydrogel printing of 3D culture chips with biofunctionalized complex 3D perfusion networks. Lab Chip 17:4273–82 [PubMed: 29116271]

228. Fairbanks BD, Schwartz MP, Bowman CN, Anseth KS. 2009 Photoinitiated polymerization of PEG-diacrylate with lithium phenyl-2,4,6-trimethylbenzoylphosphinate: polymerization rate and cytocompatibility. Biomaterials 30:6702–7 [PubMed: 19783300]

229. Torgersen J, Ovsianikov A, Mironov V, Pucher N, Qin X, et al. 2012 Photo-sensitive hydrogels for three-dimensional laser microfabrication in the presence of whole organisms. J. Biomed. Opt 17:105008 [PubMed: 23070525]

230. Ong LJY, Islam A, Das Gupta R, Iyer NG, Leo HL, Toh YC. 2017 A 3D printed microfluidic perfusion device for multicellular spheroid cultures. Biofabrication 9:045005 [PubMed: 28837043]

231. Leonhardt S, Klare M, Scheer M, Fischer T, Cordes B, Eblenkamp M. 2016 Biocompatibility of photopolymers for additive manufacturing. Curr. Dir. Biomed. Eng 2:113–16

232. Bhattacharjee N, Urrios A, Kang S, Folch A. 2016 The upcoming 3D-printing revolution in microfluidics. Lab Chip 16:1720–42 [PubMed: 27101171]

233. Zhu F, Friedrich T, Nugegoda D, Kaslin J, Wlodkowic D. 2015 Assessment of the biocompatibility of three-dimensional-printed polymers using multispecies toxicity tests. Biomicrofluidics 9:61103

234. Macdonald NP, Zhu F, Hall CJ, Reboud J, Crosier PS, et al. 2016 Assessment of biocompatibility of 3D printed photopolymers using zebrafish embryo toxicity assays. Lab Chip 16:291–97 [PubMed: 26646354]

235. Carve M, Wlodkowic D. 2018 3D-printed chips: compatibility of additive manufacturing photopolymeric substrata with biological applications. Micromachines 9:91

236. Gittard SD, Miller PR, Boehm RD, Ovsianikov A, Chichkov BN, et al. 2011 Multiphoton microscopy of transdermal quantum dot delivery using two photon polymerization-fabricated polymer microneedles. Faraday Discuss 149:171–85 [PubMed: 21413181]

237. Miller PR, Gittard SD, Edwards TL, Lopez DM, Xiao X, et al. 2011 Integrated carbon fiber electrodes within hollow polymer microneedles for transdermal electrochemical sensing. Biomicrofluidics 5:13415 [PubMed: 21522504]

238. Doraiswamy A, Jin C, Narayan RJ, Mageswaran P, Mente P, et al. 2006 Two photon induced polymerization of organic-inorganic hybrid biomaterials for microstructured medical devices. Acta Biomater 2:267–75 [PubMed: 16701886]

239. Gittard SD, Ovsianikov A, Chichkov BN, Doraiswamy A, Narayan RJ. 2010 Two-photonpolymerization of microneedles for transdermal drug delivery. Expert Opin. Drug Deliv 7:513–33 [PubMed: 20205601]

240. Al-Hiyasat AS, Darmani H, Milhem MM. 2005 Cytotoxicity evaluation of dental resin composites and their flowable derivatives. Clin. Oral Investig 9:21–25

241. Lambrecht JT, Brix F. 1990 Individual skull model fabrication for cranio facial surgery. Cleft Palate Craniofac. J 27:382–87

242. Kumar A, Ghafoor H. 2016 Rapid prototyping: a future in orthodontics. J.Orthod.Res4:1

243. Zaharia C, Gabor A-G, Gavrilovici A, Stan AT, Idorasi I, et al. 2017 Digital dentistry—3D printing applications. J. Interdiscip. Med 2:50–53
244. Nayar S, Bhuminathan S, Bhat WM. 2015 Rapid prototyping and stereolithography in dentistry. J. Pharm. Bioallied Sci 7:S216–19 [PubMed: 26015715]
245. Groth C, Graham JW, Redmond WR. 2014 Three-dimensional printing technology. J. Clin. Orthod 48:475–85 [PubMed: 25226040]
246. Darmani H, Al-Hiyasat AS, Milhem MM. 2007 Cytotoxicity of dental composites and their leached components. Quintessence Int 38:789–95 [PubMed: 17873986]
247. Peng Q, Tang Z, Liu O, Peng Z. 2015 Rapid prototyping–assisted maxillofacial reconstruction. Ann. Med 47:186–208 [PubMed: 25873231]
248. Wen X, Gao S, Feng J, Li S, Gao R, Zhang G. 2018 Chest-wall reconstruction with a customized titanium-alloy prosthesis fabricated by 3D printing and rapid prototyping. J. Cardiothorac. Surg 13:1–7 [PubMed: 29301583]
249. Toepke MW, Beebe DJ. 2006 PDMS absorption of small molecules and consequences in microfluidic applications. Lab Chip 6:1484–86 [PubMed: 17203151]
250. Regehr KJ, Domenech M, Koepse lJT, Carver KC, Ellison-Zelski SJ, et al. 2009 Biological implications of polydimethylsiloxane-based microfluidic cell culture. Lab Chip 9:2132–39 [PubMed: 19606288]
251. Delamarche E, Bernard A, Schmid H, Bietsch A, Michel B, Biebuyck H. 1998 Microfluidic networks for chemical patterning of substrate: design and application to bioassays. J. Am. Chem. Soc 120:500–8
252. Berthier E, Young EWK, Beebe D. 2012 Engineers are from PDMS-land, biologists are from polystyrenia. Lab Chip 12:1224–37 [PubMed: 22318426]
253. Jo BH, Van Lerberghe LM, Motsegood KM, Beebe DJ. 2000 Three-dimensional microchannel fabrication in polydimethylsiloxane (PDMS) elastomer. J. Microelectromechanical Syst 9:76–81
254. McDonald JC, Duffy DC, Anderson JR, Chiu DT, Wu H, et al. 2000 Fabrication of microfluidic systems in poly(dimethylsiloxane). Electrophoresis 21:27–40 [PubMed: 10634468]
255. Ren K, Dai W, Zhou J, Su J, Wu H. 2011 Whole Teflon microfluidic chips. PNAS 108:8162–66 [PubMed: 21536918]
256. Rogers CI, Pagaduan JV, Nordin GP, Woolley AT. 2011 Single-monomer formulation of polymerized polyethylene glycol diacrylate as a nonadsorptive material for microfluidics. Anal. Chem 83:6418–25 [PubMed: 21728310]
257. Nge PN, Rogers CI, Woolley AT. 2013 Advances in microfluidic materials, functions, integration, and applications. Chem. Rev 113:2550–83 [PubMed: 23410114]
258. Kuo AP, Bhattacharjee N, Lee YS, Castro K, Kim YT, Folch A. 2018 High-precision stereolithography of biomicrofluidic devices. Adv. Mater. Technol 12:1800395
259. Choi KM, Rogers JA. 2003 A photocurable poly(dimethylsiloxane) chemistry designed for soft lithographic molding and printing in the nanometer regime. J. Am. Chem. Soc 125:4060–61 [PubMed: 12670222]
260. Bhagat AAS, Jothimuthu P, Papautsky I. 2007 Photodefinable polydimethylsiloxane (PDMS) for rapid lab-on-a-chip prototyping. Lab Chip 7:1192 [PubMed: 17713619]
261. Desai SP, Taff BM, Voldman J. 2008 A photopatternable silicone for biological applications. Langmuir 24:575–81 [PubMed: 18081333]
262. Cong H, Pan T. 2008 Photopatternable conductive PDMS materials for microfabrication. Adv. Funct. Mater 18:1912–21
263. Coenjarts CA, Ober CK. 2004 Two-photon three-dimensional microfabrication of poly(dimethylsiloxane) elastomers. Chem. Mater 16:5556–58
264. Rekštytė S, Malinauskas M, Juodkazis S. 2013 Three-dimensional laser micro-sculpturing of silicone: towards bio-compatible scaffolds. Opt. Express 21:17028 [PubMed: 23938551]
265. Thrasher CJ, Schwartz JJ, Boydston AJ. 2017 Modular elastomer photo resins for digital light processing additive manufacturing. ACS Appl. Mater. Interfaces 9:39708–16 [PubMed: 29039648]

266. Patel DK, Sakhaei AH, Layani M, Zhang B, Ge Q, Magdassi S. 2017 Highly stretchable and UV curable elastomers for digital light processing based 3D printing. Adv. Mater 29:1606000
267. Xu BB, Zhang Y-L, Xia H, Dong W-F, Ding H, Sun H-B. 2013 Fabrication and multifunction integration of microfluidic chips by femtosecond laser direct writing. Lab Chip 13:1677–90 [PubMed: 23493958]
268. Selimis A, Mironov V, Farsari M. 2014 Direct laser writing: principles and materials for scaffold 3D printing. Microelectron. Eng 132:83–89
269. Kaehr B, Shear JB. 2007 Mask-directed multiphoton lithography. J. Am. Chem. Soc 129:1904–5 [PubMed: 17260997]
270. Zhou X, Hou Y, Lin J. 2015 A review on the processing accuracy of two-photon polymerization. AIP Adv 5:30701
271. LaFratta CN, Fourkas JT, Baldacchini T, Farrer RA. 2007 Multiphoton fabrication. Angew. Chem. Int. Ed. Engl 46:6238–58 [PubMed: 17654468]
272. Lee MP, Cooper GJ, Hinkley T, Gibson GM, Padgett MJ, Cronin L. 2015 Development of a 3D printer using scanning projection stereolithography. Sci. Rep 5:9875 [PubMed: 25906401]
273. Gong H, Bickham BP, Woolley AT, Nordin GP. 2017 Custom 3D printer and resin for 18μm×20μm microfluidic flow channels. Lab Chip 17:2899–909 [PubMed: 28726927]
274. Galajda P, Ormos P. 2001 Complex micromachines produced and driven by light. Appl. Phys. Lett 78:249–51
275. Galajda P, Ormos P. 2002 Rotors produced and driven in laser tweezers with reversed direction of rotation. Appl. Phys. Lett 80:4653–55
276. Xia H, Wang J, Tian Y, Chen Q-D, Du X-B, et al. 2010 Ferrofluids for fabrication of remotely controllable micro-nanomachines by two-photon polymerization. Adv. Mater 22:3204–7 [PubMed: 20603886]
277. Maruo S, Inoue H. 2006 Optically driven micropump produced by three-dimensional two-photon microfabrication. Appl. Phys. Lett 89:144101
278. Maruo S, Inoue H. 2007 Optically driven viscous micropump using a rotating microdisk. Appl. Phys. Lett 91:84101
279. He Y, Huang BL, Lu DX, Zhao J, Xu BB, et al. 2012 “Overpass” at the junction of a crossed microchannel: an enabler for 3D microfluidic chips. Lab Chip 12:3866–69 [PubMed: 22871743]
280. Wang J, He Y, Xia H, Niu LG, Zhang R, et al. 2010 Embellishment of microfluidic devices via femtosecond laser micronanofabrication for chip functionalization. Lab Chip 10:1993–96 [PubMed: 20508876]
281. Kaehr B, Shear JB. 2008 Multiphoton fabrication of chemically responsive protein hydrogels for microactuation. PNAS 105:8850–54 [PubMed: 18579775]
282. Nielson R, Kaehr B, Shear JB. 2009 Microreplication and design of biological architectures using dynamic-mask multiphoton lithography. Small 5:120–25 [PubMed: 19040218]
283. Kaehr B, Shear JB. 2009 High-throughput design of microfluidics based on directed bacterial motility. Lab Chip 9:2632–37 [PubMed: 19704977]
284. Lim TW, Son Y, Jeong YJ, Yang DY, Kong HJ, et al. 2011 Three-dimensionally crossing manifold micro-mixer for fast mixing in a short channel length. Lab Chip 11:100–3 [PubMed: 20938497]
285. Ligon SC, Liska R, Stampfl J, Gurr M, Mülhaupt R. 2017 Polymers for 3D printing and customized additive manufacturing. Chem. Rev 117:10212–90 [PubMed: 28756658]

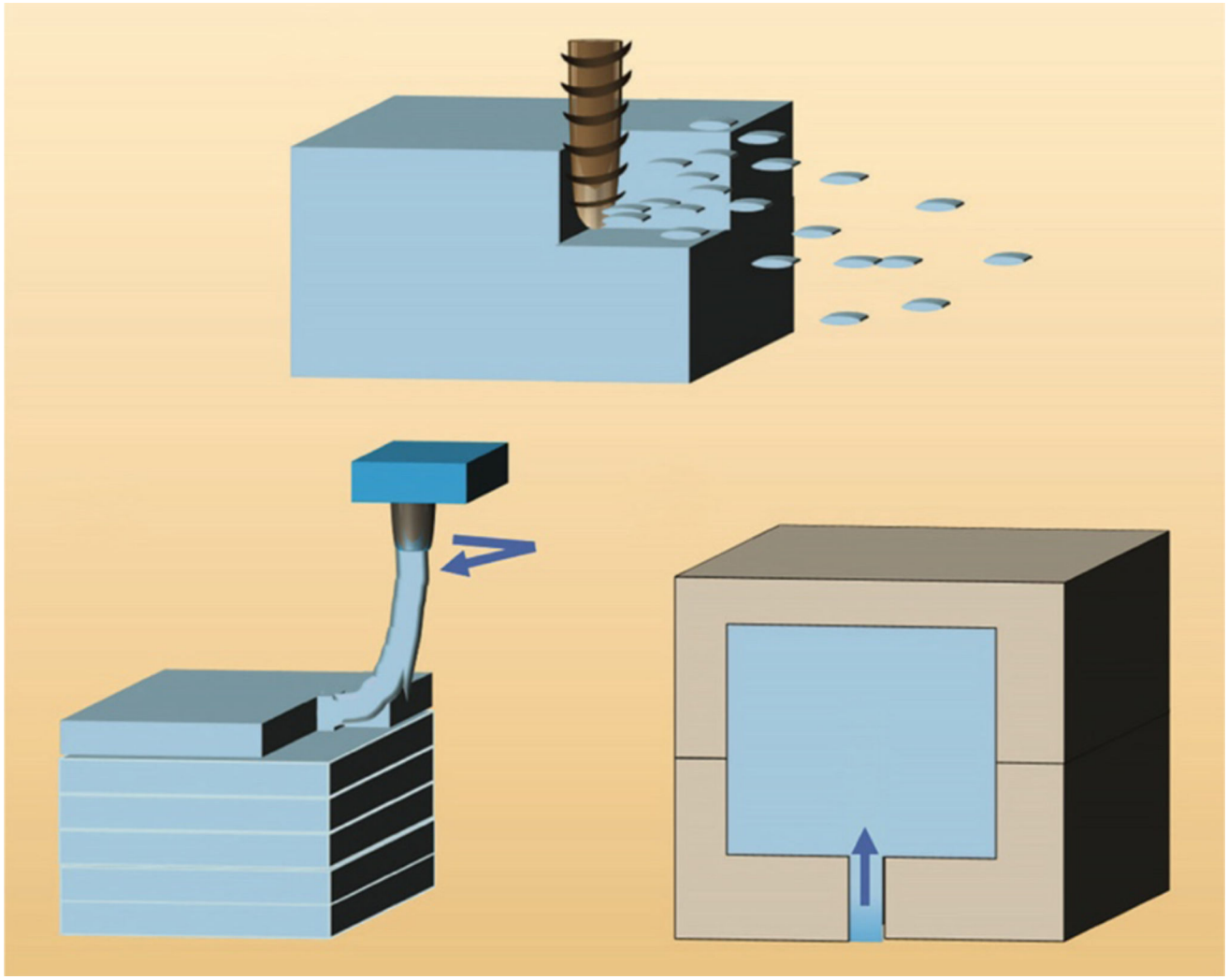

Figure 1:
Fabrication strategies used in microfluidics. (*a*) Subtractive manufacturing. (*b*) Additive manufacturing. (*c*) Molding. Figure adapted from Reference 285 with permission from the American Chemical Society.

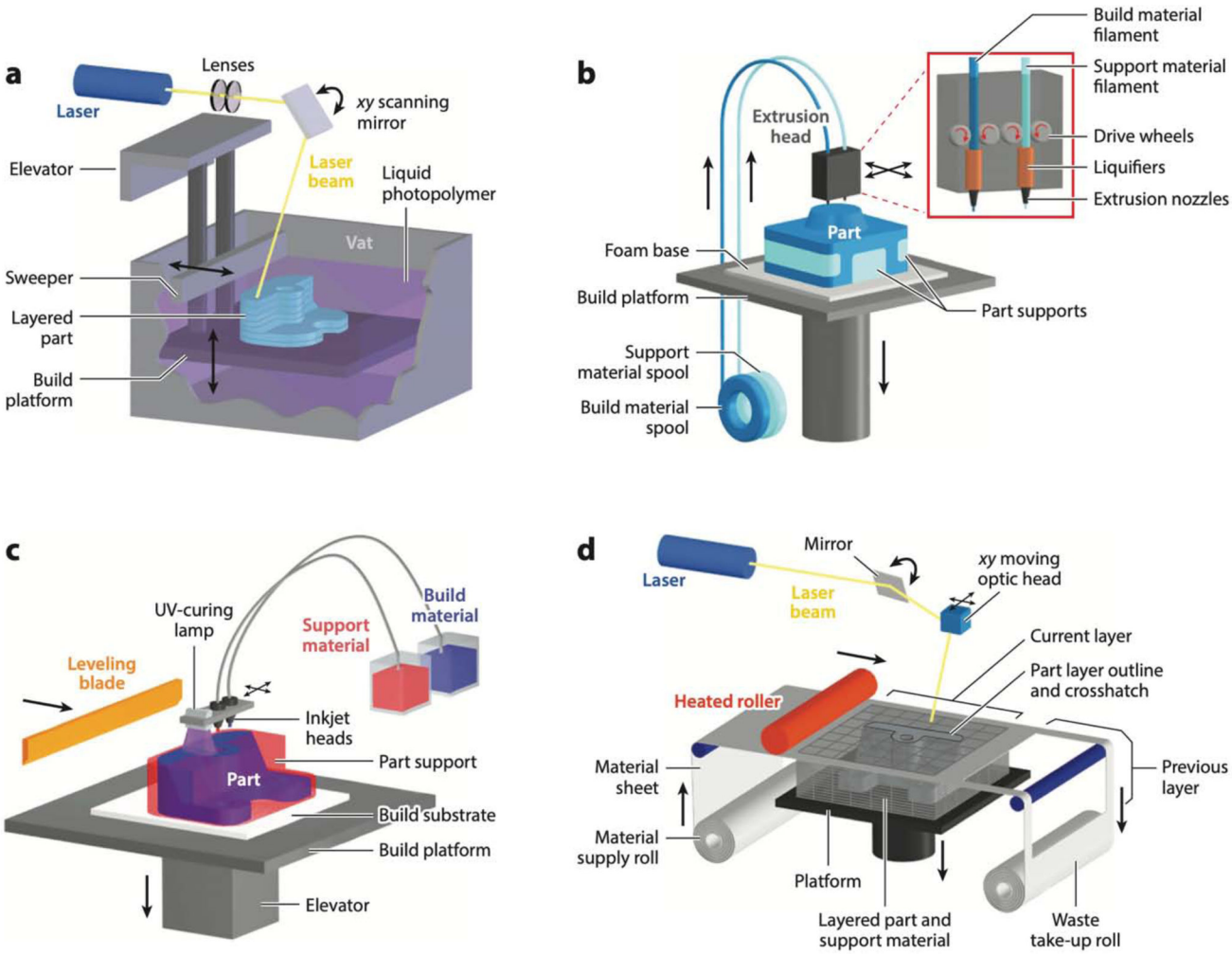

Figure 2:

Digital manufacturing techniques used in microfluidics. (*a*) Stereolithography. (*b*) Fused deposition modeling. (*c*) Photopolymer inkjet (or Polyjet) printing. (*d*) Laminated object manufacturing. Figure adapted with permission from http://www.CustomPartNet.com.

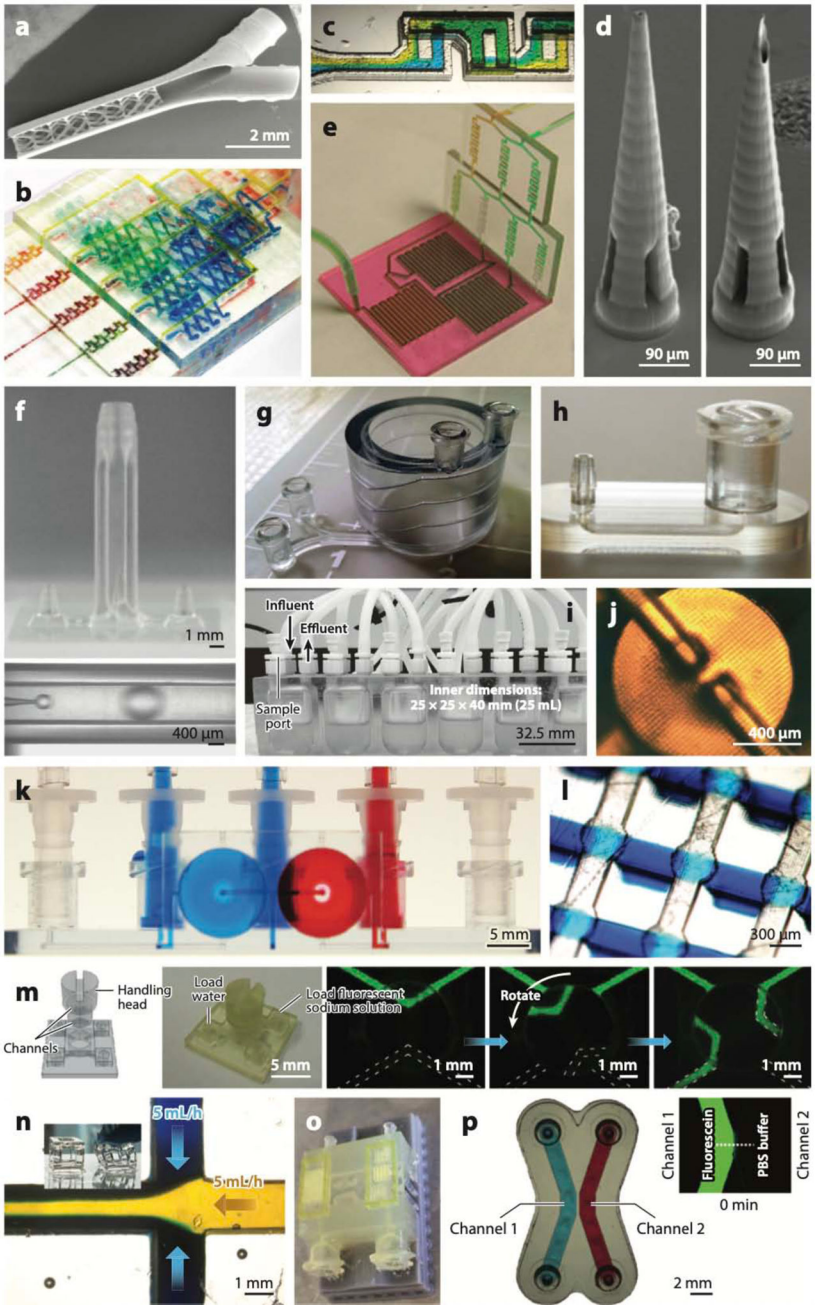

Figure 3:

Stereolithography (SL)-printed microfluidic devices. (*a*) A 3D micromixer created by digital light projection (DLP)-SL, the first 3D-printed microfluidic device. (*b*) A gradient generator, the first microfluidic device printed with a commercial desktop printer. (*c*) A 3D chaotic mixer SL-printed in poly(ethylene glycol) diacrylate with a molecular weight of 258 (PEG-DA-258), a transparent biocompatible resin. (*d*) Microneedles for transdermal drug delivery SL-printed in the biocompatible resin Ormocer. (*e*) Modular microfluidic platform. (*f*) An SL-printed droplet generator with coaxial architecture (*top*) in which monodisperse oil droplets are formed (*bottom*). (*g*) Coil-shaped microfluidic channel. (*h*) Examples of SL-

printed connectors: a male barb (*left*) and a Luer connector (*right*). (*i*) Bioreactor for bacterial culture. (*j*) Microvalve printed in PEG-DA-258. (*k*) Microfluidic switch printed in Watershed. (*l*) Array of Quake-style microvalves printed in PEG-DA-258. (*m*) SL-printed valves that are torque actuated by hand. (*n*) Flexible structures and cytocompatible microchannels printed in a poly(dimethyl siloxane) (PDMS)-like resin. (*o*) Multimaterial microfluidic perfusion channels incorporating biotinylated glyceryl-dimethacrylate microstructures. (*p*) PEG-DA-700 hydrogel barriers coprinted between and within PEG-DA-258 microchannels. Panel *a* adapted from Reference 50 with permission from the Royal Society of Chemistry (RSC). Panel *b* adapted from Reference 51 with permission from the RSC. Panel *c* adapted from Reference 258 courtesy of A. Kuo and A. Folch. Panel *d* adapted from Reference 68 with permission from Wiley. Panel *e* adapted from Reference 70 with permission from the RSC. Panel *f* adapted from Reference 74 under a Creative Commons license (CC-BY-4.0). Panel *g* adapted from Reference 45 courtesy of A. Au and A. Folch. Panel *h* courtesy of A. Au and A. Folch. Panel *i* adapted from Reference 89 with permission from R.A. Britton. Panel *j* adapted from Reference 109 with permission from the RSC. Panel *k* adapted from Reference 110 courtesy of A. Au and A. Folch. Panel *l* adapted from Reference 113 courtesy of Y.-S. Lee and A. Folch. Panel *m* adapted from Reference 114 with permission from the American Chemical Society. Panel *n* adapted from Reference 115 courtesy of N. Bhattacharjee and A. Folch. Panel *o* adapted from Reference 126 with permission from S. Turri. Panel *p* adapted from Reference 121 courtesy of Y.T. Kim and A. Folch.

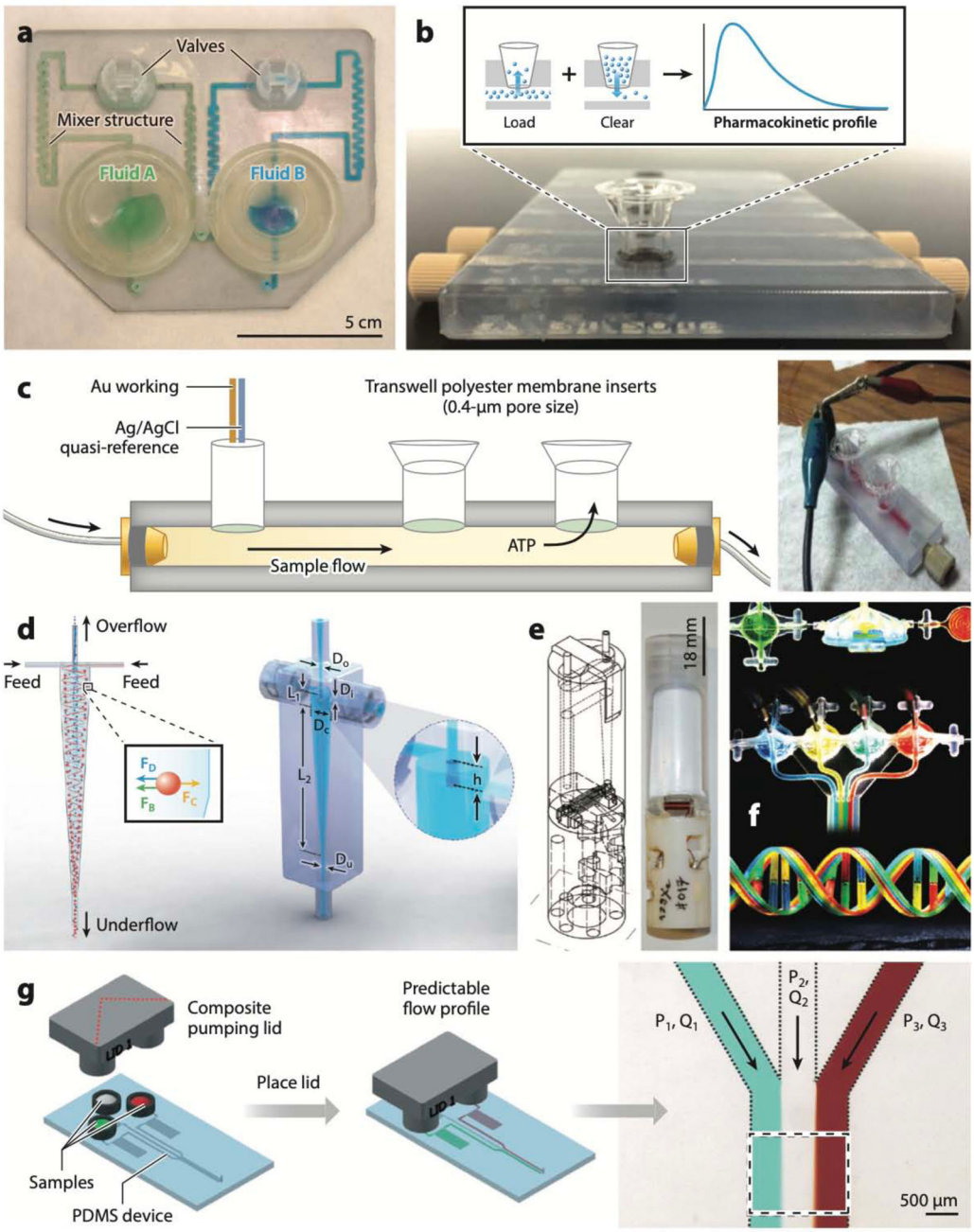

Figure 4:

Polyjet-printed microfluidic devices. (*a*) Microfluidic mixer and homogenizer for DNA and protein separations (the first Polyjet-printed microfluidic device). (*b*) Device that interfaces with commercially available Transwell membrane inserts for measuring pharmacokinetic profiles of cells. (*c*) Schematic (*left*) and photo (*right*) of a device for electrochemical detection of cellular processes, where the cells are cultured inside Transwell membrane inserts. (*d*) A minihydrocyclone for high-throughput cell separation. (*e*) Schematics (*left*) and photograph (*right*) of a bubble pump for NMR applications. (*f*) Polyjet-printed fluidic capacitors, diodes, transistors, and a multiflow controller device. (*g*) A pumping lid device

printed in two Polyjet resins (Tango Plus and Veroclear). Abbreviations: ATP, adenosine triphosphate; FB, buoyant force; FC, centrifugal force; FD, drag force; Dc, cylindrical diameter; Di, inlet diameter; Do, overflow diameter; Du, underflow diameter; L1, cylindrical length; L2, conical length; h, height of vortex finder; P1, pressure at inlet 1; P2, pressure at inlet 2; P3, pressure at inlet 3; PDMS, poly(dimethyl siloxane); Q1, volumetric flow rate for channel 1; Q2, volumetric flow rate for channel 2; Q3, volumetric flow rate for channel 3. Panel *a* adapted from Reference 129 courtesy of A. Bonyár. Panel *b* adapted from Reference 131 with permission from the American Chemical Society. Panel *c* adapted from Reference 132 with permission from the Royal Society of Chemistry (RSC). Panel *d* adapted from Reference 134 with permission from the RSC. Panel *e* adapted from Reference 136 with permission from the RSC. Panel *f* adapted from Reference 137 with permission from the RSC. Panel *g* adapted from Reference 141 with permission from the RSC.

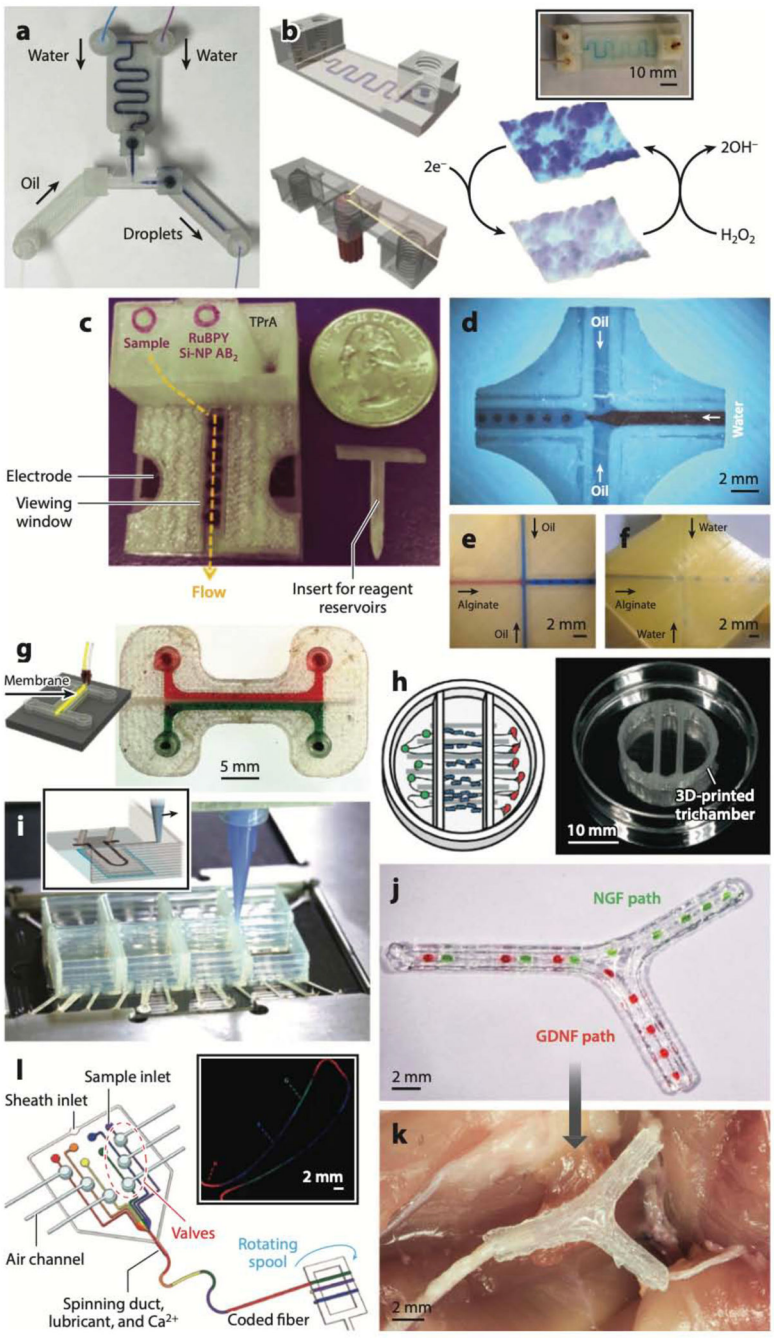

Figure 5:

Fused deposition modeling (FDM)-printed microfluidic devices. (*a*) Droplet generator. (*b*) Schematic and photo (*inset*) of device for amperometric detection of hydrogen peroxide. (*c*) Device for immunoarray-based detection of cancer protein biomarkers. (*d–f*) Droplet generators with an embedded glass observation window (*d*) or very thin polylactic acid roofs (*e*, *f*). (*g*) FDM-printed acrylonitrile butadiene styrene channels separated by an FDM-printed porous Lay–Felt barrier. (*h*) Schematic and photo of a device to study interactions among neurons, glia, and epithelial cells. (*i*) Schematic (*inset*) and photo of a cardiac organ-

on-a-chip device FDM-printed with piezoresistive, high-conductance, viscous poly(dimethyl siloxane) (PDMS) inks. (*j*, *k*) Nerve-repair FDM-printed construct that incorporates fluidic paths for nerve growth factor (NGF) and glial cell line–derived neurotrophic factor (GDNF) (*j*) and is implanted to regenerate complex peripheral nerve injuries (*k*). (*l*) PDMS device for FDM printing of silk microfibers with digitally encoded chemical composition along the fibers. Abbreviations: Si-NP, silica nanoparticle; TPrA, tripropylamine. Panel *a* adapted from Reference 164 under a Creative Commons license (CC-BY-4.0). Panel *b* adapted from Reference 166 with permission from the American Chemical Society (ACS). Panel *c* adapted from Reference 167 with permission from J.F. Rusling. Panels *d–f* adapted from Reference 171 under a Creative Commons license (CC-BY-4.0). Panel *g* adapted from Reference 172 with permission from the ACS. Panel *h* adapted from Reference 174 with permission from the Royal Society of Chemistry. Panel *i* adapted from Reference 175 with permission from J.A. Lewis and K. Parker. Panels *j* and *k* adapted from Reference 176 with permission from Wiley. Panel *l* adapted from Reference 183 with permission from A. Khademhosseini.

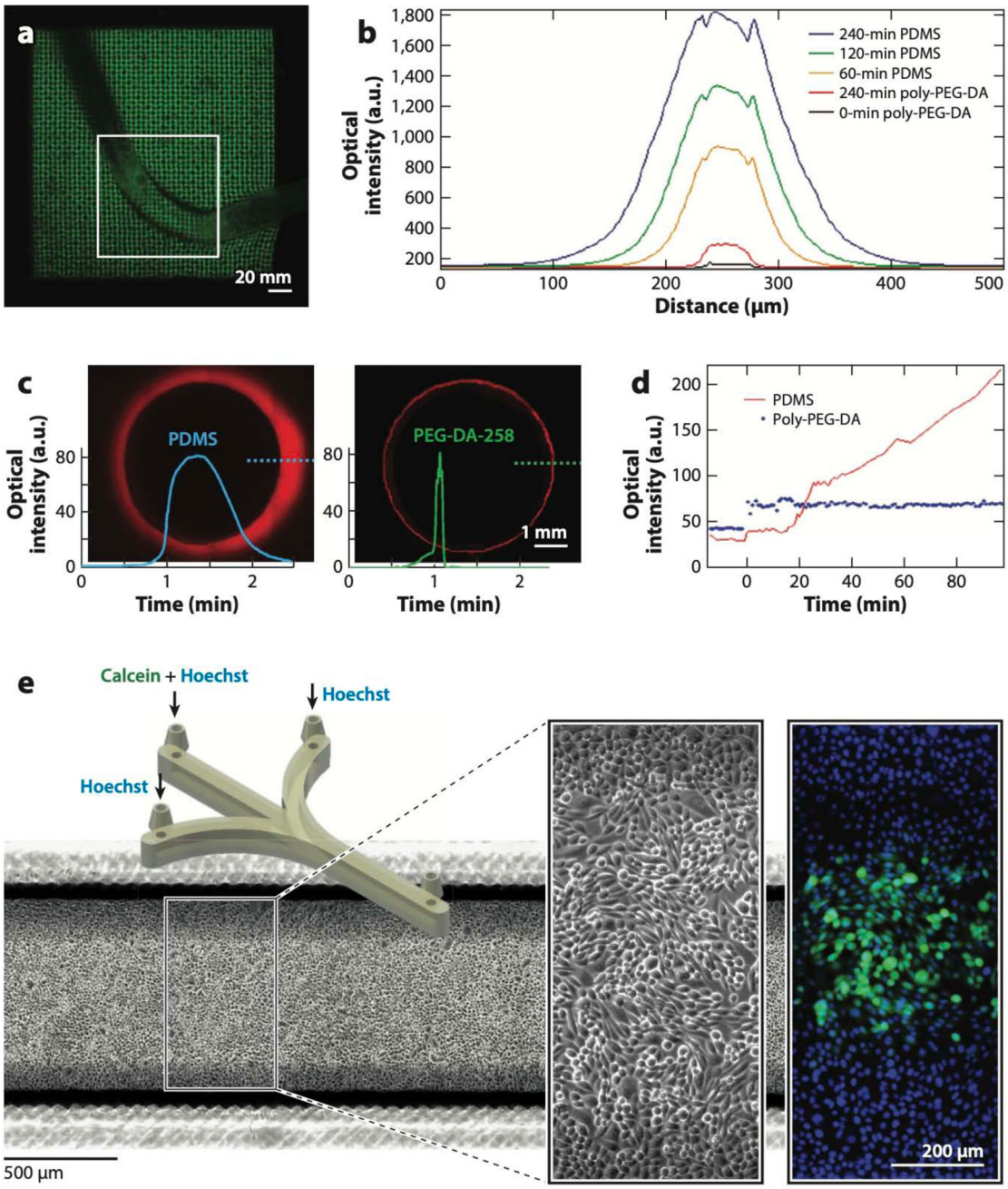

Figure 6:

Biocompatibility of digitally manufactured microfluidics. (*a*) Live *Caenorhabditis elegans* trapped in stereolithography (SL)-printed poly(ethylene glycol) diacrylate (PEG-DA)-700 hydrogel woodpile microstructures. (*b*) Comparison of the cross-sectional fluorescence profiles of molded PEG-DA-258 and poly(dimethyl siloxane) (PDMS) 50-μm-wide microchannels filled with 10 μM Rhodamine B for various amounts of time as indicated. (*c*) Comparison of the cross-sectional fluorescence profiles of thermally cured PDMS (*left*) and 3D-printed PEG-DA-258 (*right*) 5-mm-wide wells after being exposed to 1 mM Nile Red for 90 min. (*d*) Comparison of the fluorescence levels of molded PDMS and PEG-DA-258 as a

function of time during exposure to a fluorescently labeled protein (1 μg/mL FITC-BSA). (*e*) CAD design of the SL-printed microfluidic device (*left inset*) in which CHO-K1 cells were cultured and labeled with Hoechst 33342 and Calcein Green AM (*right inset*). Abbreviations: a.u., arbitrary units; CAD, computer-aided design. Panel *a* adapted from Reference 229 under a Creative Commons license (CC-BY-4.0). Panels *b* and *d* adapted from Reference 256 with permission from the American Chemical Society. Panels *c* and *e* adapted from Reference 258 courtesy of A. Kuo and A. Folch.

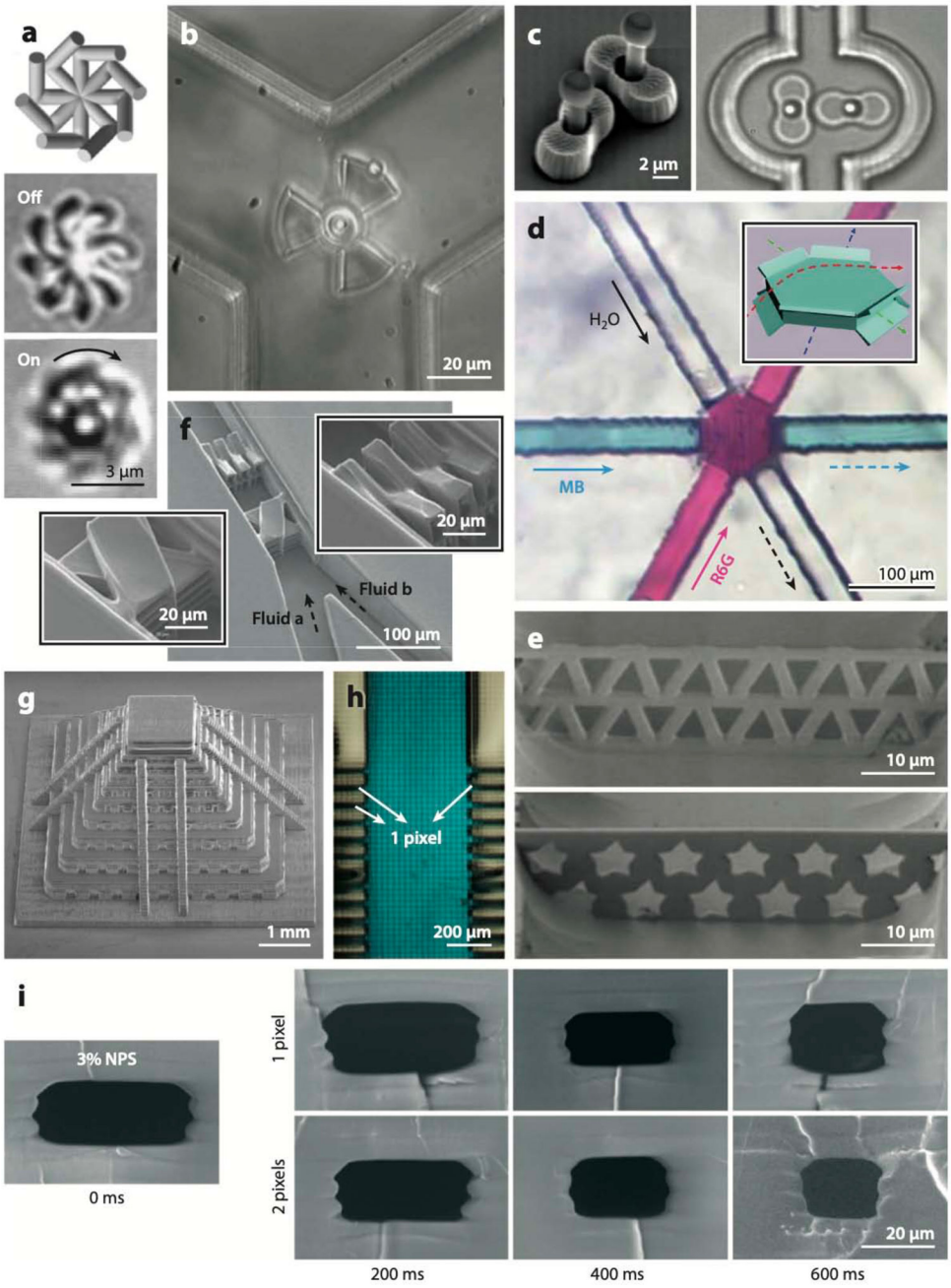

Figure 7:

Microfluidic devices printed at high resolution. (*a*) Polymer structures stereolithography (SL)-printed in the optical adhesive Norland NOA 63 (*top*) can be rotated off (*middle*) and on (*bottom*) by laser illumination. (*b*) Magnetically actuated microturbine SL-printed in a ferrofluid resin. (*c*) Micropump that is SL-printed and actuated with laser tweezers. (*d*) Fluid junction overpass fabricated by direct laser writing (DLW). (*e*) Microsieves with triangular (*top*) and pentagrammic (*bottom*) pores fabricated by DLW. (*f*) 3D micromixer featuring crisscrossing manifolds fabricated by DLW. (*g*) Micropyramid test structure SL-printed with the Dilase 3D, a high-resolution laser-based 3D printer. (*h*) A 500-μm-wide poly(ethylene

glycol) diacrylate (PEG-DA)-258 channel connected to a series of 1-mm-tall, 27-μm-wide (one pixel wide; aspect ratio, 37:1) parallel microchannels. (*i*) Microfluidic PEG-DA-258 microchannels with cross sections as small as 18 μm × 20 μm. Abbreviations: NPS, 2-nitrophenyl phenyl sulfide; MB, blue methylene blue trihydrate; R6G, Rhodamine 6G. Panel *a* adapted from Reference 274 with permission from AIP Publishing. Panel *b* adapted from Reference 267 with permission from the Royal Society of Chemistry (RSC). Panel *c* adapted from Reference 277 with permission from AIP Publishing. Panel *d* adapted from Reference 279 with permission from the RSC. Panel *e* adapted from Reference 280 with permission from the RSC. Panel *f* adapted from Reference 284 with permission from the RSC. Panel *g* adapted courtesy of Kloe, Inc. Panel *h* adapted from Reference 258 courtesy of A. Kuo and A. Folch. Panel *i* adapted from Reference 273 with permission from the RSC.